Radboud Repository

Radboud University Nijmegen

PDF hosted at the Radboud Repository of the Radboud University Nijmegen

The following full text is a preprint version which may differ from the publisher's version.

For additional information about this publication click this link.
http://hdl.handle.net/2066/124396

Please be advised that this information was generated on 2017-12-05 and may be subject to change.

EUROPEAN ORGANISATION FOR NUCLEAR RESEARCH

CERN-PPE/91-176
15 October 1991

A Study of Charged Particle Multiplicities in Hadronic Decays of the Z^0

The OPAL Collaboration

Abstract

We present an analysis of multiplicity distributions of charged particles produced in Z^0 hadronic decays. The results are based on the analysis of 82,941 events collected within 100 MeV of the Z^0 peak energy with the OPAL detector at LEP. The charged particle multiplicity distribution, corrected for initial-state radiation and for detector acceptance and resolution, was found to have a mean $< n_{ch} >= 21.40 \pm 0.02(stat.) \pm 0.43(syst.)$ and a dispersion $D = 6.49 \pm 0.02(stat.) \pm 0.20(syst.)$. The shape is well described by the Lognormal and Gamma distributions. A Negative Binomial parameterisation was found to describe the shape of the multiplicity distribution less well. A comparison with results obtained at lower energies confirms the validity of KNO(-G) scaling up to LEP energies. A separate analysis of events with low sphericity, typically associated with two-jet final states, shows the presence of features expected for models based on a stochastic production mechanism for particles. In all cases, the features observed in the data are well described by the Lund parton shower model JETSET.

(Submitted to Zeitschrift für Physik C)

The OPAL Collaboration

P.D. Acton[25], G. Alexander[23], J. Allison[16], P.P. Allport[5], K.J. Anderson[9], S. Arcelli[2], P. Ashton[16], A. Astbury[a], D. Axen[b], G. Azuelos[18,c], G.A. Bahan[16], J.T.M. Baines[16], A.H. Ball[17], J. Banks[16], G.J. Barker[13], R.J. Barlow[16], J.R. Batley[5], G. Beaudoin[18], A. Beck[23], J. Becker[10], T. Behnke[27], K.W. Bell[20], G. Bella[23], P. Berlich[10], S. Bethke[11], O. Biebel[3], U. Binder[10], I.J. Bloodworth[1], P. Bock[11], B. Boden[3], H.M. Bosch[11], S. Bougerolle[b], B.B. Brabson[12], H. Breuker[8], R.M. Brown[20], R. Brun[8], A. Buijs[8], H.J. Burckhart[8], P. Capiluppi[2], R.K. Carnegie[6], A.A. Carter[13], J.R. Carter[5], C.Y. Chang[17], D.G. Charlton[8], P.E.L. Clarke[25], I. Cohen[23], W.J. Collins[5], J.E. Conboy[15], M. Cooper[22], M. Couch[1], M. Coupland[14], M. Cuffiani[2], S. Dado[22], G.M. Dallavalle[2], S. De Jong[8], P. Debu[21], L.A. del Pozo[5], M.M. Deninno[2], A. Dieckmann[11], M. Dittmar[4], M.S. Dixit[7], E. Duchovni[26], G. Duckeck[11], I.P. Duerdoth[16], D.J.P. Dumas[6], G. Eckerlin[11], P.A. Elcombe[5], P.G. Estabrooks[6], E. Etzion[23], F. Fabbri[2], M. Fincke-Keeler[a], H.M. Fischer[3], D.G. Fong[17], C. Fukunaga[24], A. Gaidot[21], O. Ganel[26], J.W. Gary[4], J. Gascon[18], R.F. McGowan[16], N.I. Geddes[20], C. Geich-Gimbel[3], S.W. Gensler[9], F.X. Gentit[21], G. Giacomelli[2], V. Gibson[5], W.R. Gibson[13], J.D. Gillies[20], J. Goldberg[22], M.J. Goodrick[5], W. Gorn[4], C. Grandi[2], F.C. Grant[5], J. Hagemann[27], G.G. Hanson[12], M. Hansroul[8], C.K. Hargrove[7], P.F. Harrison[13], J. Hart[5], P.M. Hattersley[1], M. Hauschild[8], C.M. Hawkes[8], E. Heflin[4], R.J. Hemingway[6], R.D. Heuer[8], J.C. Hill[5], S.J. Hillier[1], D.A. Hinshaw[18], C. Ho[4], J.D. Hobbs[8], P.R. Hobson[25], D. Hochman[26], B. Holl[8], R.J. Homer[1], A.K. Honma[a], S.R. Hou[17], C.P. Howarth[15], R.E. Hughes-Jones[16], R. Humbert[10], P. Igo-Kemenes[11], H. Ihssen[11], D.C. Imrie[25], A.C. Janissen[6], A. Jawahery[17], P.W. Jeffreys[20], H. Jeremie[18], M. Jimack[2], M. Jobes[1], R.W.L. Jones[13], P. Jovanovic[1], D. Karlen[6], K. Kawagoe[24], T. Kawamoto[24], R.K. Keeler[a], R.G. Kellogg[17], B.W. Kennedy[15], C. Kleinwort[8], D.E. Klem[19], T. Kobayashi[24], T.P. Kokott[3], S. Komamiya[24], L. Köpke[8], F. Kral[8], R. Kowalewski[6], H. Kreutzmann[3], J. von Krogh[11], J. Kroll[9], M. Kuwano[24], P. Kyberd[13], G.D. Lafferty[16], F. Lamarche[18], W.J. Larson[4], J.G. Layter[4], P. Le Du[21], P. Leblanc[18], A.M. Lee[17], M.H. Lehto[15], D. Lellouch[26], P. Lennert[11], C. Leroy[18], J. Letts[4], S. Levegrün[3], L. Levinson[26], S.L. Lloyd[13], F.K. Loebinger[16], J.M. Lorah[17], B. Lorazo[18], M.J. Losty[7], X.C. Lou[12], J. Ludwig[10], M. Mannelli[8], S. Marcellini[2], G. Maringer[3], A.J. Martin[13], J.P. Martin[18], T. Mashimo[24], P. Mättig[3], U. Maur[3], J. McKenna[a], T.J. McMahon[1], J.R. McNutt[25], F. Meijers[8], D. Menszner[11], F.S. Merritt[9], H. Mes[7], A. Michelini[8], R.P. Middleton[20], G. Mikenberg[26], J. Mildenberger[6], D.J. Miller[15], R. Mir[12], W. Mohr[10], C. Moisan[18], A. Montanari[2], T. Mori[24], M.W. Moss[16], T. Mouthuy[12], B. Nellen[3], H.H. Nguyen[9], M. Nozaki[24], S.W. O'Neale[8,d], B.P. O'Neill[4], F.G. Oakham[7], F. Odorici[2], M. Ogg[6], H.O. Ogren[12], H. Oh[4], C.J. Oram[e], M.J. Oreglia[9], S. Orito[24], J.P. Pansart[21], B. Panzer-Steindel[8], P. Paschievici[26], G.N. Patrick[20], S.J. Pawley[16], P. Pfister[10], J.E. Pilcher[9], J.L. Pinfold[26], D. Pitman[a], D.E. Plane[8], P. Poffenberger[a], B. Poli[2], A. Pouladdej[6], E. Prebys[8], T.W. Pritchard[13], H. Przysiezniak[18], G. Quast[27], M.W. Redmond[9], D.L. Rees[1], K. Riles[4], S.A. Robins[13], D. Robinson[8], A. Rollnik[3], J.M. Roney[9], E. Ros[8], S. Rossberg[10], A.M. Rossi[2,f], M. Rosvick[a], P. Routenburg[6], K. Runge[10], O. Runolfsson[8], D.R. Rust[12], S. Sanghera[6], M. Sasaki[24], A.D. Schaile[10], O. Schaile[10], W. Schappert[6], P. Scharff-Hansen[8], P. Schenk[a], H. von der Schmitt[11], S. Schreiber[3], J. Schwiening[3], W.G. Scott[20], M. Settles[12], B.C. Shen[4], P. Sherwood[15], R. Shypit[b], A. Simon[3], P. Singh[13], G.P. Siroli[2], A. Skuja[17], A.M. Smith[8], T.J. Smith[8], G.A. Snow[17], R. Sobie[g], R.W. Springer[17], M. Sproston[20], K. Stephens[16], H.E. Stier[10,†], R. Ströhmer[11], D. Strom[9], H. Takeda[24], T. Takeshita[24], P. Taras[18], S. Tarem[26], P. Teixeira-Dias[11], N.J. Thackray[1], T. Tsukamoto[24], M.F. Turner[5], G. Tysarczyk-Niemeyer[11], D. Van den plas[18], R. Van Kooten[8], G.J. VanDalen[4], G. Vasseur[21], C.J. Virtue[19], A. Wagner[27], C. Wahl[10], J.P. Walker[1], C.P. Ward[5], D.R. Ward[5], P.M. Watkins[1], A.T. Watson[1], N.K. Watson[8], M. Weber[11], P. Weber[6], S. Weisz[8], P.S. Wells[8], N. Wermes[11], M. Weymann[8], M.A. Whalley[1], G.W. Wilson[21], J.A. Wilson[1], I. Wingerter[8], V-H. Winterer[10], N.C. Wood[16], S. Wotton[8], T.R. Wyatt[16], R. Yaari[26], Y. Yang[4,h], G. Yekutieli[26], M. Yurko[18], I. Zacharov[8], W. Zeuner[8], G.T. Zorn[17].

[1]School of Physics and Space Research, University of Birmingham, Birmingham, B15 2TT, UK
[2]Dipartimento di Fisica dell' Università di Bologna and INFN, Bologna, 40126, Italy
[3]Physikalisches Institut, Universität Bonn, D-5300 Bonn 1, FRG
[4]Department of Physics, University of California, Riverside, CA 92521 USA
[5]Cavendish Laboratory, Cambridge, CB3 0HE, UK
[6]Carleton University, Dept of Physics, Colonel By Drive, Ottawa, Ontario K1S 5B6, Canada
[7]Centre for Research in Particle Physics, Carleton University, Ottawa, Ontario K1S 5B6, Canada
[8]CERN, European Organisation for Particle Physics, 1211 Geneva 23, Switzerland
[9]Enrico Fermi Institute and Department of Physics, University of Chicago, Chicago Illinois 60637, USA
[10]Fakultät für Physik, Albert Ludwigs Universität, D-7800 Freiburg, FRG
[11]Physikalisches Institut, Universität Heidelberg, Heidelberg, FRG
[12]Indiana University, Dept of Physics, Swain Hall West 117, Bloomington, Indiana 47405, USA
[13]Queen Mary and Westfield College, University of London, London, E1 4NS, UK
[14]Birkbeck College, London, WC1E 7HV, UK
[15]University College London, London, WC1E 6BT, UK
[16]Department of Physics, Schuster Laboratory, The University, Manchester, M13 9PL, UK
[17]Department of Physics and Astronomy, University of Maryland, College Park, Maryland 20742, USA
[18]Laboratoire de Physique Nucléaire, Université de Montréal, Montréal, Quebec, H3C 3J7, Canada
[19]National Research Council of Canada, Herzberg Institute of Astrophysics, Ottawa, Ontario K1A 0R6, Canada
[20]Rutherford Appleton Laboratory, Chilton, Didcot, Oxfordshire, OX11 0QX, UK
[21]DPhPE, CEN Saclay, F-91191 Gif-sur-Yvette, France
[22]Department of Physics, Technion-Israel Institute of Technology, Haifa 32000, Israel
[23]Department of Physics and Astronomy, Tel Aviv University, Tel Aviv 69978, Israel
[24]International Centre for Elementary Particle Physics and Dept of Physics, University of Tokyo, Tokyo 113, and Kobe University, Kobe 657, Japan
[25]Brunel University, Uxbridge, Middlesex, UB8 3PH UK
[26]Nuclear Physics Department, Weizmann Institute of Science, Rehovot, 76100, Israel
[27]Universität Hamburg/DESY, II Inst. für Experimental Physik, 2000 Hamburg 52, FRG

[a]University of Victoria, Dept of Physics, P O Box 3055, Victoria BC V8W 3P6, Canada
[b]University of British Columbia, Dept of Physics, 6224 Agriculture Road, Vancouver BC V6T 1Z1, Canada
[c]Also at TRIUMF, Vancouver, Canada V6T 2A3
[d]On leave from Birmingham University, Birmingham B15 2TT, UK
[e]Univ of Victoria, Dept of Physics, P.O. Box 1700, Victoria BC V8W 2Y2, Canada and TRIUMF, Vancouver, Canada V6T 2A3
[f]Present address: Dipartimento di Fisica, Università della Calabria and INFN, 87036 Rende, Italy
[g]University of British Columbia, Dept of Physics, 6224 Agriculture Road, Vancouver BC V6T 2A6, Canada and IPP, McGill University, High Energy Physics Department, 3600 University Str, Montreal, Quebec H3A 2T8, Canada
[h]On leave from Research Institute for Computer Peripherals, Hangzhou, China
[†]deceased 25th March 1991

1 Introduction

The multiplicity distribution of charged hadrons produced in high energy collisions is one of the basic observables characterizing multiparticle final states. It has been extensively studied both experimentally and theoretically [1]. Data are available for a large variety of interactions (hadron-hadron, lepton-hadron, electron-positron collisions). Charged multiplicity in e^+e^- annihilations can be used to test QCD analytic predictions as well as fundamental statistical hypotheses about the multiparticle production process in high energy interactions. The charged multiplicity is usually studied for the whole event and for limited phase space regions: this latter to reduce possible effects from charge and momentum conservation constraints.

In this paper we present the results of an analysis of charged particle multiplicity distributions from e^+e^- annihilations into hadrons at the Z^0 peak, obtained with the OPAL detector at LEP. Results are presented for both the whole event and a single event hemisphere. Our results are compared with those obtained by other experiments at the same and at lower centre-of-mass energies as well as with the expectations of QCD based parton shower models and other phenomenological models.

In Section 2 we describe the detector components relevant to this analysis and the experimental event- and track-selection criteria adopted. Section 3 contains a description of the procedure used to unfold the data while in Section 4 we discuss the systematic uncertainties affecting our measurements. Section 5 is devoted to the presentation of the fully corrected charged multiplicity distributions followed by a discussion of the dependence of the mean charged multiplicity and of the normalised moments on the energy, of the shape of the multiplicity distributions and of the results obtained for data samples selected according to the event sphericity. The results are summarized in Section 6.

2 The OPAL Detector and Data Selection

The data used in this work were recorded with the OPAL detector at the CERN e^+e^- collider, LEP. The analysis is based on the entire data sample accumulated during the 1990 run at a centre-of-mass energy of 91.2 GeV (about 106,000 multihadronic events collected within 100 MeV of the Z^0 peak, corresponding to an integrated luminosity of approximately 3.5 pb^{-1}).

OPAL is a multipurpose apparatus covering almost the entire solid angle around the interaction region. It consists of a system of central tracking chambers enclosed by a solenoidal magnet which provides a highly uniform axial magnetic field of 0.435 T, surrounded by a time-of-flight system, an electromagnetic calorimeter with a presampler, a hadron calorimeter and an outer shell of muon chambers. Two forward detectors provide a luminosity measurement by counting low angle Bhabha events. The OPAL detector and its trigger system have been described in detail elsewhere [2]. Here we briefly summarize only those features relevant to this study.

A cylindrical coordinate system is defined in OPAL, with the z axis following the electron beam direction, r in the plane perpendicular to the z axis and θ and ϕ being the polar and azimuthal angles with respect to the z axis. The measurement of the trajectories and momenta of the charged particles is performed with a central tracking system consisting of three sets of chambers :

1. A high precision drift chamber for vertex reconstruction ("Vertex chamber") divided into 36 sectors with 12 axial and 6 stereo wires each. The (r,ϕ) track coordinate is measured with a single hit resolution of $\sigma_{r\phi} \approx 50$ μm and the z-coordinate with a precision of $\sigma_z \approx 700$ μm.

2. A large volume drift chamber ("Jet chamber") for high precision measurements in the plane perpendicular to the beam axis. It is divided into 24 azimuthal sectors, providing up to 159 measurements per track over a radius of about 1.8 m , with a precision of $\sigma_{r\phi} \approx 130\mu$m and $\sigma_z \approx 6$ cm. The double track resolution is about 3 mm in the r-ϕ plane. In addition the energy loss for each particle is measured with a precision of $\sigma(dE/dx)/(dE/dx) \approx 3.8\%$ allowing a good statistical separation of the various kinds of particles over a wide momentum range.

3. An outer layer of drift chambers ("Z-chambers") for accurate position measurements along the beam direction. It yields up to six measurements with a single hit resolution of $\sigma_z \approx 300$ μm.

The complete system allows detection of charged particles over 98% of the full solid angle. The track finding efficiency is close to 100% for tracks in the region $|\cos\theta| < 0.92$. The momentum resolution achieved for charged particles is:

$$\sigma_{p_T}/p_T \approx \sqrt{0.02^2 + (0.0018 \times p_T/(\mathrm{GeV}/c))^2}\ ,$$

where p_T is the momentum component transverse to the beam direction. The mean polar angle resolution is about 1.5 mrad.

The electromagnetic calorimeter consists of a barrel and two endcap arrays of lead glass blocks. Each block subtends a solid angle of approximately 40×40 mrad^2, with a thickness of over 24 radiation lengths in the barrel region and typically 22 radiation lengths in the endcaps. Electromagnetic energy deposits ("clusters") are formed from one or more contiguous blocks which contain signals above the threshold of 20 MeV and 50 MeV for the barrel and endcaps, respectively. The total solid angle covered by the electromagnetic calorimeter is 98% of 4π.

Multihadronic decays of the Z^0 were triggered by a system based on independent trigger signals from the central tracking devices (Vertex chamber and Jet chamber), the time-of-flight detector and the electromagnetic barrel and endcap calorimeters. This high redundancy allowed an accurate measurement of the overall trigger efficiency from the data. It was found to be greater than 99.9% within the acceptance of the analysis cuts. More details about the triggering and multihadronic decay candidate selection can be found in [3].

In the present analysis, additional selection criteria, based on charged track and electromagnetic energy cluster information, were applied to obtain a sample of well contained and well measured multihadronic events and to reduce further the contamination from background processes. We considered only events for which all the components of the central tracking system and of the electromagnetic calorimeter were fully operational (93.4% of the initial event sample). Charged tracks were accepted only if they had:

- At least 40 measured points recorded in the Jet chamber (corresponding to a minimum track length of 40 cm).
- A distance of closest approach to the interaction point of less than 5 cm (d_0) in the direction perpendicular to the beam axis and less than 30 cm (z_0) along the beam axis.
- A momentum component transverse to the beam direction, p_T, larger than 150 MeV/c.
- A measured polar angle w.r.t. the beam direction in the range 20° to 160°.

A reconstructed track was occasionally assigned an unphysical momentum, i.e. considerably larger than the beam energy. Those tracks (about 0.07% of the total and adequately reproduced by the detector simulation program) were not used in the analysis.

Electromagnetic clusters were accepted only if they had:

- At least 100 MeV of energy, if they appeared in the barrel.
- At least 200 MeV of energy, spread over two or more adjacent lead-glass blocks, if they appeared in the endcaps.

The multihadron event sample was selected considering only the accepted tracks and clusters, and the events were required to have :

a) A total energy deposited in the lead-glass blocks of at least 20% of the centre-of-mass energy.

b) A total visible momentum, defined as the sum of the charged particle momenta p_i measured in the central detector, $\sum_i \mid p_i \mid > 15$ GeV/c.

c) The polar angle of the thrust axis, θ_T, computed from the charged track momenta, in the range $30° \leq \theta_T \leq 150°$.

d) At least 5 charged tracks and at least 8 clusters.

e) An energy imbalance, R_{bal}, along the beam direction which satisfied the condition

$R_{bal} \equiv \mid \sum(E_{clus} \cdot \cos\theta_c) \mid / \sum E_{clus} < 0.65$,

where θ_c is the polar angle of the cluster.

f) At least one hemisphere, defined by a plane perpendicular to the thrust axis, in which the effective mass associated to the charged particle system was greater than 2 GeV/c^2. Pion masses were assigned to the observed tracks.

g) The principal thrust value, computed from the charged track momenta, smaller than 0.9975.

Cuts a),b) and c) define well contained multihadron candidates. Cuts a),b),c),d) and e) provide a powerful rejection against background to multihadrons from other processes ($\tau^+\tau^-$ and two-photon hadronic events, beam-gas and beam-wall interactions, showers from large angle Bhabha events). The remaining background events, estimated to be about 0.1% at this level, come mostly from $\tau^+\tau^-$ decays and are concentrated at low multiplicity. Although they correspond to only one part in a thousand of the total sample, their contribution to the content of the lowest multiplicity bins is not negligible. From a Monte Carlo study we estimated a contamination of about 50% and 40% for an observed track multiplicity of n_{ch}=5 and n_{ch}=6, respectively, dropping to about 4% at a track multiplicity of n_{ch}=7. For this reason we further reduce the contamination from $\tau^+\tau^-$ and possible residual events produced by Bhabha electrons showering in the beam-pipe making use of cuts f) and g). These cuts were found to have essentially no effect on the genuine multihadronic events and are very efficient in removing the background, reducing the $\tau^+\tau^-$ contamination to 7% and 5% for track multiplicities of five and six, respectively.

The above mentioned cuts reduced the data sample to 82,941 events, with an estimated total residual background of about 0.026% from $\tau^+\tau^-$ pairs. The background from all the other sources is negligible.

The criteria adopted for the selection of multihadronic event candidates were based on a Monte Carlo study of the OPAL detector response to Z^0 decays into hadronic final states. With this selection, we estimated the detection efficiency to be 84.5% $\pm$ 0.5%. More details about the simulation of hadronic events in OPAL can be found in the next section. The background contamination of the multihadron sample was estimated from a study of events generated with the Monte Carlo programs

KORALZ [4] for τ pairs, BABAMC [5] for large angle Bhabha events and VERMASEREN [6] for two-photon events. Those events were passed through the full detector simulation, reconstruction and analysis programs. The τ rejection criteria were also tested on the 1990 OPAL experimental τ candidate sample and were found to have essentially the same rejection power as predicted by the Monte Carlo.

3 Simulation of Hadronic Events and Correction Procedure

The charged multiplicity distributions observed experimentally need to be corrected for several effects. It is necessary to correct for the loss of particles due to the geometrical acceptance and resolution of the tracking system as well as for the efficiency of the track finding algorithm. On the other hand, e^+e^- pairs from photon conversions and nuclear interactions of hadrons in the material of the inner part of the detector produce spurious tracks that should not be considered. The multihadron sample was selected by requiring the events to satisfy certain conditions and a small bias in multiplicity is introduced. In addition, QED initial-state radiation produces a bias (although very small at the Z^0 peak) due to an effective reduction of the centre-of-mass energy and, consequently, of the mean multiplicity.

The final multiplicity distributions to be presented in Section 5 were corrected for all the above mentioned effects. The correction procedure was based on simulated multihadronic decays of the Z^0 generated with the Lund parton shower model JETSET 7.2 [7] with five flavours and string fragmentation. The model was used with a set of optimised parameters determined from a study of global event shape variables performed by OPAL [8]. The unfolding method is the same as that used in a recent work by the TASSO Collaboration [12].

Two distinct steps were performed to correct the measured unnormalised multiplicity distributions. The first step was to correct for effects introduced by the detector (geometrical acceptance and resolution, contamination due to particle interactions in the material) and by the reconstruction program (track finding inefficiencies and other imperfections). For this purpose a sample of about 185,000 multihadronic events including QED initial-state radiation was processed through the OPAL detector simulation program [9]. This program contains a detailed description of the experimental apparatus, a simulation of the interactions with the detector materials and a simulation of the response of each detector component. The simulated raw data were written in the same format as the experimental ones and were processed by the same reconstruction and analysis programs as the data. In Fig.1(a,b) we show the experimentally observed multiplicity distributions for the whole event and for a single hemisphere, respectively. The algorithm which defines the single hemisphere distributions is described below. The corresponding distributions for the simulated event sample are plotted as histograms showing a good agreement.

For each Monte Carlo event that passed the selection criteria presented in Section 2, the number of observed tracks n_o (with distribution $N^{MC}_{obs.}(n_o)$) was compared to the number of tracks actually generated n_g (with distribution $N^{MC}_{true}(n_g)$). The number of events with n_g generated tracks when n_o have been observed, divided by the total number of events observed with n_o tracks, determines a correction matrix $M(n_g, n_o)$ whose elements are defined as

$$M(n_g, n_o) = \frac{\text{No. of events with } n_g \text{ tracks generated when } n_o \text{ were observed}}{\text{No. of events with } n_o \text{ tracks observed}} .$$

The element $M(n_g, n_o)$ of this unfolding matrix is the fraction of events which have been observed with n_o tracks and that had a "true" multiplicity n_g. The observed multiplicity distribution $N^{MC}_{obs}(n_o)$

is thus related to the "true" multiplicity distribution $N^{MC}_{true}(n_g)$ by

$$N^{MC}_{true}(n_g) = \sum_{n_o} M(n_g, n_o) \cdot N^{MC}_{obs}(n_o) \quad . \tag{1}$$

In this measurement, the "true" multiplicity of an event is defined as the total number of all promptly produced charged particles and those produced in the decays of particles with lifetimes shorter than 3×10^{-10} sec. This means that charged decay products from K^0_s and weakly decaying heavy-mesons (D,F,...) and baryons (Λ, Σ,...) as well as from their antiparticles are included in the definition, regardless of how far away from the interaction point the decay actually occurred.

The contributions of K^0_s, Λ, $\overline{\Lambda}$ etc. to the charged multiplicity may be subtracted by computing the unfolding matrices keeping the relevant particles stable at the Monte Carlo generation level. In this way the identification of their decay products is not necessary, but the procedure relies on how well the model used to unfold the data describes their production and decay. A recent work published by OPAL [11] demonstrates that JETSET describes the K^0_s production rate very well. The contribution to the mean charged multiplicity is predicted to be about 1.5 units for K^0_s, 0.5 units for Λ and $\overline{\Lambda}$ and negligible (less than 0.02 units) for the remaining shortlived neutral particle decays. For brevity, when referring to Λ particles we always mean Λ and $\overline{\Lambda}$.

A second step in the correction procedure was taken to correct for the effects of event selection and QED initial-state radiation. A set of correction factors C_F was computed from Monte Carlo by comparing the "true" multiplicity distribution $N^{MC}_{true}(n_g)$ defined above, after normalisation to the number of events $N^{MC-true}_{total}$ in the sample, to the corresponding distribution $N^{MC}_{fixed}(n_g)$ obtained from the same event generator for a fixed centre-of-mass energy (no initial state radiation)

$$C_F(n_g) = \frac{N^{MC}_{true}(n_g)/N^{MC-true}_{total}}{N^{MC}_{fixed}(n_g)/N^{MC-fixed}_{total}} \quad . \tag{2}$$

The correction factor C_F were found to be close to 1.

Finally, the unfolding matrix M and the set of correction factors C_F were applied to the experimentally observed multiplicity distributions $N^{exp}_{obs}(n_o)$, to yield the corrected multiplicity distributions $N^{exp}_{cor}(n)$

$$N^{exp}_{cor}(n) = C_F(n) \cdot \sum_{n_o} M(n, n_o) \cdot N^{exp}_{obs}(n_o) \quad . \tag{3}$$

One should note that this kind of unfolding procedure is model dependent and provides a reliable correction of the data only if the multiplicity distributions observed at the detector level for real events are well reproduced by the fully simulated events. This is the case for our analysis as shown in Fig.1(a,b).

The unfolding procedure described above was applied to the experimentally observed multiplicity distributions for the whole event and for a single hemisphere. The event was divided into two hemispheres by a plane perpendicular to the thrust axis computed from the measured charged track momenta for real events and from the generated charged particle momenta for simulated events. For each event, one of the two hemispheres was chosen randomly. Because of the requirement that five or more observed tracks be present in an event, the values $N^{exp}_{cor}(n)$ for n_{ch}=2 and n_{ch}=4 for the whole event distributions were not derived from the data but were taken instead from the Monte Carlo predictions.

4 Systematic Uncertainties

In this section we present a discussion of the sources of systematic errors. Where appropriate, the entire analysis as outlined in section 3 was repeated to test the influence of a systematic effect on the final results. In the following, we define the reference distribution to be the multiplicity distribution obtained using JETSET with the standard OPAL detector simulation program and selection criteria given in section 2. We observed that some of the systematic effects left the shape of the multiplicity distribution essentially unchanged, but led to a shift of its mean value. In this case, a straightforward bin-by-bin difference between the reference distribution and the others would overestimate the point-to-point systematic error, because of the high level of anti-correlation between the errors calculated this way below and above the mean value. Therefore, to estimate the point-to-point systematic uncertainty, each normalised distribution, obtained by repeating the entire analysis under a different condition, was locally parameterised by polynomial functions [1]. Each of the parameterised distributions was compared to the reference one after having been shifted along the multiplicity axis by an amount equal to the difference between the mean values of the two (which never exceeded 0.35 units). The difference between a particular bin content of the reference distribution and the height of the shifted parameterised distribution for the same bin defined the systematic error for that bin, while the systematic error for the mean equaled the amount of the shift. We have taken as an estimate of the overall uncertainty all the differences, arising from the sources of systematic errors considered, added in quadrature.

Several possible sources of systematic errors have been studied:

1. In order to investigate the effects produced by possible differences between the actual detector performance and that represented in the simulation program, samples of multihadronic events, generated according to the JETSET parton shower model, were produced with a modified detector simulation. The values of the relevant smearing parameters of the tracking chamber simulation, like the spatial resolution along the beam direction and the double hit resolution, were varied over a reasonably wide range, and the corresponding event samples were reconstructed and analysed by the same programs used for the analysis. The unfolding matrices and correction factors obtained from each sample were used to correct the experimental distribution. The differences observed when comparing these distributions with the reference one were evaluated as previously described and taken as representative of this systematic uncertainty.

2. We tested the stability of our results using a different definition of well measured tracks and a different selection of multihadronic event candidates. Track quality cuts, like minimum track length, transverse momentum, polar angle, distance of closest approach to the interaction point (d_0, z_0), as well as event selection cuts, like minimum thrust polar angle and visible energy, were varied. Again, a new set of unfolding matrices and correction factors was computed and applied to the real data, processed with the corresponding selection criteria. The systematic uncertainties were estimated as previously described.

3. The correction procedure relies on the QCD event generator. In order to study a possible model dependence of our measurement, we compared our reference results with those obtained using the HERWIG parton shower model generator version 5.0 [10]. About 100,000 multihadronic decays of the Z^0 , generated with the HERWIG model with parameters optimised as described in [8], were passed through the detector simulation, reconstruction and analysis programs. As shown in Fig.1(c,d) this model provides a reasonably good description of our data, although not as good as the one provided by JETSET. The differences between the two model predictions

[1] The need of a parameterisation with a continuous function is determined by the fact that we are dealing with discrete distributions and, as will be described later, we want to compute the value of a distribution for a non integer value.

are particularly relevant in the tails of the multiplicity distribution, because the distribution predicted by HERWIG is slightly broader than that predicted by JETSET. The uncertainties associated to the first and to the last few points of the distribution are dominated by this source of systematic error.

4. The data were collected over a period of several months during which the detector performance was always carefully monitored. Nevertheless random unknown problems may have occurred. In order to check the detector stability over such an extended period of time, the global sample was divided in twelve roughly equal parts and the mean multiplicity and dispersion of the distributions were calculated separately. The chi-squared probabilities when comparing the twelve values to a constant (the weighted mean multiplicity and dispersion) were found to be about 15% and 40%, respectively, providing satisfactory evidence that the observed deviations were consistent with statistical fluctuations.

5. The estimated background from $\tau^+\tau^-$ decays into hadrons was discussed in Section 2. Since it is small, we did not explicitly correct the multiplicity distributions for this contamination but we increased the uncertainty associated to the bin contents at multiplicities n_{ch}=5 and n_{ch}=6 in the observed distribution for the whole event by an amount equivalent to the estimated number of background events. An explicit correction would have produced a completely negligible effect on the various moments.

6. The fraction of events with a total charged multiplicity n_{ch}=2 and n_{ch}=4 was not measured but taken from the JETSET model prediction after normalisation to the number of events in the data. As a systematic uncertainty we have taken the difference between the JETSET and the HERWIG predictions for these multiplicities. We checked that the mean multiplicity, the dispersion and the other moments remain essentially unchanged if the content of the first two bins of the distribution is not considered in the calculations.

The non-negligible contributions to the systematic uncertainty on each moment of the distribution are listed separately in Table 1. The overall systematic uncertainty was determined by adding them in quadrature.

5 Results

The fully corrected normalised charged particle multiplicity distributions for the whole event and for the single hemisphere are presented in Table 2(a,b). For each multiplicity n, the fraction of corrected events in percent, $P(n)$, the statistical uncertainty (first) and the systematic uncertainty (second) are given. Statistical uncertainties take into account the finite number of events both in the data and in the Monte Carlo samples. Table 2(a) refers to distributions where the charged decay products of K^0_s, Λ, etc. are included, while Table 2(b) refers to distributions where these contributions have been removed, as explained in Section 3.

The distributions presented in Table 2(a) are shown in Fig. 2. The plotted experimental uncertainties contain the statistical and systematic errors added in quadrature. In the same figure we also plot the predictions from JETSET. The data are well described by the model, with a χ^2 value per degree of freedom of 26.3/25 for the whole event [2] and 19.8/35 for the single hemisphere. For HERWIG we obtain the values 70.5/25 and 23.9/35, respectively. Only statistical uncertainties are used in these χ^2 calculations.

[2] Points at multiplicity 2 and 4 have not been considered

In Table 3 we present a summary of our corrected results for the mean charged multiplicity $< n_{ch} >$, the dispersion $D = (< n_{ch}^2 > - < n_{ch} >^2)^{\frac{1}{2}}$, the ratio $< n_{ch} > /D$ and the normalised multiplicity moments $C_k =< n_{ch}^k > / < n_{ch} >^k$ calculated for both the whole event and the single hemisphere. The quoted errors are statistical and systematic, respectively. In the values presented in Table 3(a), contributions from K_s^0 and Λ decays are included while they are excluded in those presented in Table 3(b) .

When not stated otherwise, the analysis and the results presented below refer to the distributions containing K_s^0 and Λ charged decay products (see Table 2a).

5.1 Mean Charged Multiplicity

The corrected mean charged multiplicity measured is $< n_{ch} >= 21.40 \pm 0.02(stat.) \pm 0.43(syst.)$. It agrees well with the number previously published by OPAL [8] (the overall uncertainty of the new analysis is about a factor of two smaller) and with those measured by MARK II [13], ALEPH [14], DELPHI [15,16] and L3 [17] at the same centre-of-mass energy.

In Fig. 3 we show the energy dependence of $< n_{ch} >$ measured by this and by other experiments at e^+e^- colliders [12-25]. In this compilation only published results have been included. The plotted errors are the overall uncertainties on $< n_{ch} >$ computed by adding in quadrature the published statistical and systematic errors. The values measured at LEP and at SLC were taken at the same energy; their positions in Fig.3 are slightly displaced for a clearer graphical presentation.

One should note that the Collaborations $\gamma\gamma 2$ at ADONE and MARK I at SPEAR, providing a total of 56 measurements in the energy range from 1.4 GeV to 7.8 GeV, do not explicitly quote systematic errors on $< n_{ch} >$ in their published papers. In a recent paper from TASSO [12] a systematic uncertainty similar to that estimated for their own measurement (about 4%) was attributed to these measurements in a fit to the data over the whole energy range. However, there are indications that the actual uncertainty is larger for these data. For example, measurements by LENA [20] and JADE [22] at similar energies several years later, quote an experimental systematic uncertainty of 10% and 7%, respectively. In Fig. 3 we have assigned a systematic error of 5% to these points but allow it to be as large as 10% when making fits to the mean charged multiplicity over the complete energy range, as discussed below.

A number of phenomenological models have been proposed to describe the evolution with energy of the mean charged multiplicity . Various parameterisations were fitted to the data plotted in Fig. 3. The form

$$< n_{ch} >= a \cdot s^b \tag{4}$$

was first suggested by Fermi within the context of a phase space model [26] and has also been derived from the fireball and hydrodynamical models for hadron-hadron interactions [27]. A fit of (4) to the data yields $a = 2.220 \pm 0.027$ and $b = 0.252 \pm 0.002$ with $\chi^2 = 132.2$ for 82 degrees of freedom. In a recent work [28], it was pointed out that all published models predicting a power law for the energy dependence of the mean multiplicity obtain the result (4) in the limit of a continuous distribution. For discrete distributions a more appropriate form is, according to [28]:

$$< n_{ch} >= \beta \cdot s^\alpha - 1 \, . \tag{5}$$

A fit to the data using (5) yields $\beta = 2.979 \pm 0.029$ and $\alpha = 0.222 \pm 0.002$ with $\chi^2 = 183.7$ for 82 degrees of freedom.

A fit according to the empirical relation

$$< n_{ch} >= a + b \cdot \ln(s) + c \cdot \ln^2(s) \ , \tag{6}$$

proposed for hadronic interactions to describe the data up to the highest energies [29], yields $a = 3.297 \pm 0.091$, $b = -0.394 \pm 0.056$ and $c = 0.263 \pm 0.007$ with $\chi^2 = 69.1$ for 81 degrees of freedom.

More recently, a form motivated by perturbative QCD calculations of the parton evolution in a leading-log approximation was proposed [30]:

$$< n_{ch} >= a + b \cdot exp(c \cdot \sqrt{\ln(s/Q_0^2)}\ ) \ . \tag{7}$$

A fit of this form to the data taking $Q_0 = 1$ GeV, where Q_0 is a cut-off parameter in the perturbative calculations associated with the onset of hadronisation effects, yields $a = 2.418 \pm 0.082$, $b = 0.113 \pm 0.012$ and $c = 1.712 \pm 0.035$ with $\chi^2 = 93.6$ for 81 degrees of freedom.

Based on the χ^2 values obtained, one might conclude that forms (4) and (5) are disfavoured with respect to the others. However it is clear from Fig. 3 that the contribution to the χ^2, when fitting Eq. (5) to the data, for example, is dominated by the low energy points (below 8 GeV). One should remember that the systematic uncertainty attributed to the low energy points was arbitrarily chosen to be 5%, and may be underestimated. Furthermore, at such low energies, resonances and threshold effects may produce small-scale fluctuations. If the assumed systematic uncertainty of the data measured by the $\gamma\gamma 2$ and MARK I Collaborations is increased from 5% to 10% and the fits of Eq. (4), (5), (6) and (7) to the data are repeated, we find that the parameter values remain the same within the quoted errors, while the χ^2 values per degree of freedom drop to 64.5/82, 70.8/82, 35.8/81 and 54/81, respectively. We have also checked that the four parameterisations give essentially indistinguishable results when they are fitted to data measured at energies above the upsilon threshold. Our conclusion is that none of these four parameterisations can be definitively excluded by the presently available data.

The energy dependence of the mean multiplicity of hadrons produced in hard processes has been calculated in perturbative QCD including next-to-leading log corrections [31,32] and has the form:

$$< n_{ch} >= a \cdot \alpha_s^b \cdot exp(c/\sqrt{\alpha_s})(1 + O(\sqrt{\alpha_s})) \ , \tag{8}$$

where a is a normalisation constant that cannot be calculated in the framework of perturbation theory. According to reference [32], the validity of Eq. (8) is restricted to energies above the upsilon threshold and we therefore fitted (8) to the data for centre-of-mass energies above 10 GeV. For the running coupling constant we used the expression:

$$\frac{\alpha_s(s)}{4\pi} = \frac{1}{\beta_0 ln(s/\Lambda^2)} - \frac{\beta_1 lnln(s/\Lambda^2)}{\beta_0^3 ln^2(s/\Lambda^2)} \ . \tag{9}$$

For five active quark flavours, the parameters β_0, β_1, b and c have the values $\beta_0 = 7.67$, $\beta_1 = 38.67$, $b = 0.49$ and $c = 2.27$ [32]. Neglecting the $O(\sqrt{\alpha_s})$ term, one can treat a and Λ as free parameters. The fitted Λ then becomes a process-dependent quantity, expected to be close to $\Lambda_{\overline{MS}}$ if the $O(\sqrt{\alpha_s})$ term is small. Eq.(8) is found to provide a good description of the energy dependence of the mean charged multiplicity, the best fit parameters being $a = 0.065 \pm 0.010$ and $\Lambda = 136 \pm 50$ MeV, yielding $\chi^2 = 5.6$ for 22 degrees of freedom.

5.2 Moments of the Multiplicity Distributions

The energy dependence of $< n_{ch} > /D$ and of the moments C_k is shown in Fig. 4 for the whole event and in Fig. 5 for a single hemisphere. The decay products from K_s^0 and Λ are included. The plotted errors are the statistical and systematic uncertainties added in quadrature for all the experiments except AMY, for which only statistical errors are available. For clarity, the two LEP points are plotted at slightly different energies. Our results are in good agreement with those published by the DELPHI Collaboration at the same energy [15] and confirm the observation that the measured values of these quantities do not change appreciably up to LEP energies.

The ratio $R = (< n_{ch} > /D)^{Whole}_{event}/(< n_{ch} > /D)^{Single}_{Hem.}$ is expected to be equal to $\sqrt{2}$, for events with a two-jet topology, if the jets are produced independently and if the multiplicities are uncorrelated in the two jets [33]. Measurements by the TASSO collaboration [12] of this quantity show values close to $\sqrt{2}$ (1.35 ± 0.03, 1.35 ± 0.03, 1.34 ± 0.01 and 1.35 ± 0.02 at 14, 22, 34.8 and 43.6 GeV, respectively), but do not show any convergence to this value [34]. The TASSO measurement was recently supported by that of the DELPHI Collaboration [15], who measured the value of $R = 1.34 \pm 0.01 \pm 0.04$. Our result for this ratio is $R = 1.36 \pm 0.01 \pm 0.02$, in the case where K_s^0 and Λ decays are included, and $R = 1.35 \pm 0.01 \pm 0.02$ if K_s^0 and Λ decay products are removed. The JETSET model prediction is 1.36 in both cases.

The above results are derived from an inclusive sample of multihadronic final states rather than from a pure two-jet sample, whereas the expectation of $R = \sqrt{2}$ refers to this last case. It is well known that at LEP energies most of the events show a characteristic two-jet event structure. The fraction of events with significant hard gluon bremsstrahlung, however, is appreciable. For these events the single hemisphere is not a good approximation of a clean single-jet. We separately analysed samples of events selected using cuts on the sphericity variable. We repeated the analysis on four samples of events for which the measured sphericity S was smaller than 0.30, 0.15, 0.09 and 0.03, respectively. Our detector resolution limits the analysis to $S > 0.03$ [8]. By requiring the events to have a smaller sphericity, one suppresses the fraction of events containing hard gluon bremsstrahlung. After these cuts the four samples are reduced to about 95%, 86%, 76% and 48% of the total, respectively. The corresponding fully simulated Monte Carlo samples, used in the unfolding procedure, were obtained by applying the same selection criteria. All these samples were found to reproduce the data satisfactorily. After correcting the observed distributions, our measured values for the ratio R were determined to be 1.38 ± 0.01, 1.40 ± 0.01, 1.41 ± 0.01 and 1.42 ± 0.02 for events having a measured sphericity smaller than 0.30, 0.15, 0.09 and 0.03. These values are plotted in Fig. 6. The overall systematic uncertainty in each of these measurements is estimated to be 0.02. Very similar values for these ratios are also obtained at the detector level, i.e. using the uncorrected distributions, giving confidence that the unfolding procedure does not introduce significant distortions. The measurements show that the ratio R increases with increasing purity of the two-jet sample, and approaches a value compatible with $\sqrt{2}$ within errors. The JETSET model predictions, based on parton shower with string fragmentation, are in complete agreement with our experimental results, being 1.37, 1.39, 1.40 and 1.42 for events having a sphericity smaller than 0.30, 0.15, 0.09 and 0.03, respectively.

5.3 Shape of the Multiplicity Distribution

Several parameterisations have been proposed to describe the shape of the charged multiplicity distribution (for a review see for example [35]). An energy independent form was presented in 1972 by Koba, Nielsen and Olesen [36]. Assuming the validity of Feynman scaling [37], they derived the asymptotic result (KNO-scaling) that multiplicity distributions measured at different energies should

coincide when plotted using the scaled variables $z = n_{ch}/ < n_{ch} >$ and $\Psi(z) =< n_{ch} > \cdot P(n_{ch})$. The concept of multiplicity scaling, originally formulated for asymptotic energies and thus to be considered as an approximation when applied to the available data, was mathematically reformulated by Golokhvastov [38] in order to be applicable also at finite energies. This formulation, known as KNO-G scaling, should be more appropriate when testing possible scaling properties of the multiplicity and should provide a better description of the data particularly at lower energies.

Multiplicity distributions in e^+e^- annihilations at different centre-of-mass energies have been often compared using the KNO and the KNO-G variables. As observed in hadronic interactions, KNO scaling was found to hold in the energy range from $\approx$ 10 GeV to 44 GeV , while significant deviations were observed at lower energies [12,22] [3]. Using the more appropriate KNO-G formulation it was shown that scaling in multiplicity is also observed at the lowest energies [28,39], while its validity was recently extended up to KEK [25] and LEP energies [15,28]. In hadronic interactions both formulations seem to fail in describing the data at the highest SPS Collider energies [40].

In Fig.7 and Fig.8 we show a graphical test of KNO and KNO-G scaling. In these figures, our corrected charged multiplicity distribution measured for the whole event is compared to the distributions measured by other experiments at different centre-of-mass energies using the scaled variables $z = n_{ch}/ < n_{ch} >$ and $\Psi(z) =< n_{ch} > \cdot P(n_{ch})$ in the first case, and the variables $S_n = \sum_{k=n}^{\infty} P_k$ and $\tilde{z} = n_{ch}/ < \tilde{n}_{ch} >$ in the second case. $< \tilde{n}_{ch} >$ is an average continuous multiplicity approximated by the simple formula $< \tilde{n}_{ch} >=< n_{ch} > +0.5$ [28]. Our data do not show appreciable deviations from the shape of the lower energy measurements, confirming the validity of the scaling up to the LEP energy.

The KNO scaling function is often taken to be a "Γ" distribution,

$$\Psi(z) = \frac{K^K}{\Gamma(K)} z^{K-1} e^{-Kz} , \tag{10}$$

where $z = n_{ch}/ < n_{ch} >$ is the scaled multiplicity and K is a free parameter. This form was fitted to our multiplicity distribution for the whole event and the result is displayed in Fig. 9, both on a linear and logarithmic scale. The deviations of the fit from the measured points are shown in units of the overall experimental uncertainties in the small uppermost plot in Fig. 9. The fit yields the value $K = 10.86 \pm 0.17$ with a χ^2 of 3.7 for 24 degrees of freedom. For the fit, the overall errors defined as in Fig. 2 were considered and the two points at multiplicities $n_{ch} = 2$ and $n_{ch} = 4$ were not used.

Recently it was shown that the scaling properties observed in multiplicity distributions can be derived by assuming a scale invariant branching process to be the basis of the multiparticle production mechanism [28]. This approach has the appealing feature that the scaling property of the multiplicity distribution follows from the statistical nature of the scale invariant branching process rather than being related to Feynman scaling, which is known to be broken by gluon radiation. In this model the multiplicity distribution P_n is related to a continuous density function $f(\tilde{n})$ by $P_n = \int_n^{n+1} f(\tilde{n}) d\tilde{n}$, where $f(\tilde{n})$ is described by a Lognormal distribution. Following [41], we fitted our discrete distribution for the whole event to the integrated scaling function of the Lognormal shape

$$P_n = \int_{n/<\tilde{n}>}^{(n+1)/<\tilde{n}>} \frac{N}{\sqrt{2\pi}\sigma} \cdot \frac{1}{\tilde{z}+c} exp\left(-\frac{[ln(\tilde{z}+c)-\mu]^2}{2\sigma^2}\right) d\tilde{z} , \tag{11}$$

where $\tilde{z} = n/ < \tilde{n} >$ is the scaled multiplicity and σ, μ and c are parameters of which only two are independent because of normalisation conditions. The two strongly correlated parameters σ and μ can be expressed as a function of the parameter c and the dispersion D as follows [41]

[3] For this reason KNO scaling is sometimes referred to as approximate scaling.

$$\sigma = \sqrt{ln\left[\left(\frac{D}{1+c}\right)^2 + 1\right]} \qquad ; \qquad \mu = ln(c+1) - \sigma^2/2 \ . \tag{12}$$

From this fit we obtain $c = 0.373 \pm 0.068$ and $D = 0.290 \pm 0.002$ with a χ^2 of 6.0 for 23 degrees of freedom. The result is presented in Fig. 10.

Another well known parameterisation for the multiplicity distribution is the Negative Binomial Distribution (NBD)

$$P_n = \frac{k(k+1)...(k+n-1)}{n!}\left(\frac{< n >}{< n > +k}\right)^n \left(\frac{k}{< n > +k}\right)^k \ , \tag{13}$$

where $< n >$ and k are free parameters. There are several phenomenological approaches leading to a NBD type of multiplicity distribution (for a review see [35]). The dispersion D of the Negative Binomial Distribution is related to k and $< n >$ by

$$\frac{D^2}{< n >^2} = \frac{1}{< n >} + \frac{1}{k} \ . \tag{14}$$

The "clan" picture [42], for example, provides an interpretation for k, linking it to the average number of particles in one "clan" and the average number of "clans" [4]. It is also interesting to note that in a next to leading-log order QCD calculation [43] the moments of the multiplicity distribution are found to be very close to those of a NBD.

We have fitted the Negative Binomial Distribution to our corrected multiplicity distributions for the whole event and for the single hemisphere. From this fit we obtain for the whole event the parameter values $< n_{ch} >= 21.28 \pm 0.07$ and $k = 21.34 \pm 0.71$, with a χ^2 of 31.7 for 23 degrees of freedom and $< n_{ch} >= 10.63 \pm 0.04$ and $k = 14.5 \pm 0.04$, with a χ^2 of 101 for 33 degrees of freedom for the single hemisphere. These results are presented in Fig. 11 and in Fig. 12. For the whole event, the description of the data is not as good as the one provided by the Gamma or by the Lognormal distributions. The deviations from the measured points, shown in the top part of each figure, are systematically larger over the full multiplicity range. For the single hemisphere, the quality of the NBD fit is considerably worse than it is for the whole event.

As a last study we considered the simplest proposed distribution, the Poissonian distribution, which would be valid if the final state particles were emitted independently as is expected in pure longitudinal phase space models and in a geometrical model of multiparticle production [33]. The HRS experiment [23] reported that the charged multiplicity distribution at $\sqrt{s} = 29$ GeV was well described by a "modified Poisson" form (MPD)

$$\mathrm{MPD}(n) = \begin{cases} 2\frac{<n>^n e^{-<n>}}{n!} & \text{if } n = \text{even} \\ 0 & \text{if } n = \text{odd} \ . \end{cases} \tag{15}$$

At somewhat higher energies, however, the TASSO experiment [12] observed significant deviations from this form, the deviations becoming even more significant at KEK energies [25]. Again, these studies were performed on the inclusive data sample, whereas the predictions of the geometrical model [33] are strictly valid for two-jet events only [5].

Our results from the study of $R = (< n_{ch} > /D)^{Whole}_{event}/(< n_{ch} > /D)^{Single}_{Hem.}$ (Fig. 6) suggest a tendency toward the independent production of particles populating the two event hemispheres for

[4] In a recent experimental analysis performed in restricted central rapidity intervals [16] it was shown that the average number of clans per event and per unit of rapidity is approximately the same as at lower energies.

[5] Unfortunately it is not completely clear what the authors of [33] mean by a two-jet event.

events with a cleaner two-jet structure. Thus, in addition to our inclusive data set, we also fitted a Poissonian form to the multiplicity distributions obtained for samples of events selected using cuts on the sphericity variable.

In Fig. 13 we show the whole event multiplicity distributions, both on a linear and logarithmic scale, for the inclusive sample (a) and for samples of events for which the measured sphericity S is smaller than 0.15 (b) and 0.03 (c). In this figure only the statistical errors are shown. Superimposed on the data points are plotted the fitted modified Poissonian (continuous line) and, for comparison, also the fitted NBD (dash-dotted line). For increasingly "cleaner" two-jet events (smaller sphericity) the shape of the multiplicity distribution becomes narrower and more symmetric, leading to the result that the Poissonian distribution describes the data better. This same trend, although not as striking, is also observed for the NBD [6]. Again, we find that the JETSET parton shower model reproduces the multiplicity distributions quite well.

6 Summary and Conclusions

In this paper a study of charged particle multiplicities in multihadronic decays of the Z^0 has been presented.

The whole event mean charged particle multiplicity and dispersion are measured to be $< n_{ch} >= 21.40 \pm 0.02(stat.) \pm 0.43(syst.)$ and $D = 6.49 \pm 0.02(stat.) \pm 0.20(syst.)$, respectively [7].

The energy dependence of the mean charged multiplicity, studied over the entire energy range available from e^+e^- experiments, is well parameterised by the forms

$$< n_{ch} >= a + b \cdot \ln(s) + c \cdot \ln^2(s)$$

as suggested from high energy hadronic interactions and

$$< n_{ch} >= a + b \cdot exp(c \cdot \sqrt{\ln(s/Q_0^2)})$$

as motivated by QCD calculations in the leading log approximation.
The power law

$$< n_{ch} >= \beta \cdot s^{\alpha} - 1$$

as suggested by a scale invariant branching model for particle production describes the data less well. This conclusion however depends on the systematic uncertainties which are assumed for the measurements from e^+e^- experiments below the upsilon threshold. The three parameterisations are essentially equivalent if the data are fitted above this threshold. The form

$$< n_{ch} >= a \cdot \alpha_s^b \cdot exp(c/\sqrt{\alpha_s})$$

[6] A similar observation was presented in [44] where the analysis was performed separately for 2,3 and 4-jet event topologies (defined according to a jet finder algorithm) and studied in restricted rapidity intervals.

[7] Charged decay products from K_s^0 and Λ are included.

(with α_s as in Eq. 9) derived from QCD in next-to-leading order, describes the energy dependence of mean multiplicity well, the best value for the process dependent parameter Λ being 136 ± 50 MeV.

The validity of KNO(-G) scaling is confirmed at $\sqrt{s} = 91.2$ GeV, in agreement with the results in [15], but with higher statistics. The shape of the multiplicity distribution for the whole event is equally well described by the Gamma and the Lognormal distributions, while the Negative Binomial parameterisation is less adequate. The NBD description of the single hemisphere distribution is quite poor.

In addition to the inclusive data sample, we also analysed separately events for which hard gluon emission was suppressed. This was achieved by progressively selecting samples of events with smaller sphericity. For these clean "two-jet" events, features predicted in the context of simple stochastic models for multiparticle production have been observed. The measured quantity $R = (< n_{ch} > /D)^{Whole}_{event}/(< n_{ch} > /D)^{Single}_{Hem.}$, for example, approaches the predicted value of $\sqrt{2}$ as the events become more collimated, while the shape of the multiplicity distribution becomes narrower and more symmetric, tending to a Poisson-like form.

In all cases, the features observed in this analysis can be well reproduced by the Lund parton shower model JETSET, with string fragmentation. HERWIG, with cluster fragmentation, also describes the general features of the data, but less well.

7 Acknowledgements

It is a pleasure to thank the SL Division for the efficient operation of the LEP accelerator and their continuing close cooperation with our experimental group. In addition to the support staff at our own institutions we are pleased to acknowledge the Department of Energy, USA, National Science Foundation, USA, Science and Engineering Research Council, UK, Natural Sciences and Engineering Research Council, Canada, Israeli Ministry of Science, Minerva Gesellschaft, Japanese Ministry of Education, Science and Culture (the Monbusho) and a grant under the Monbusho International Science Research Program, American Israeli Bi-national Science Foundation, Direction des Sciences de la Matière du Commissariat à l'Energie Atomique, France, Bundesministerium für Forschung und Technologie, FRG, and the A.P. Sloan Foundation.

References

[1] For recent extensive reviews see, for example:
Multiparticle Dynamics (Festschrift for L. Van Hove), A. Giovannini and W. Kittel (eds.), World Scientific, Singapore 1990;
G. Giacomelli, Int. J. Mod. Phys. A5 (1990) 223;
Hadronic Multiparticle Production, P. Carruthers (ed.), World Scientific, Singapore 1990;
A. K. Wróblewski, Warsaw University preprint IFD/10/1990; Plenary talk at the 25^{th} Int. Conf. on High Energy Physics, Singapore, Aug. 1990.

[2] OPAL Collaboration, K. Ahmet *et al.*, Nucl. Instr. and Meth. A305 (1991) 275;
M. Arignon *et al.*, "The Trigger System of the OPAL Experiment at LEP", CERN-PPE/91-32 (1991), Submitted to Nucl. Instr. and Meth.

[3] OPAL Collaboration, M. Akrawy *et al.*, Phys. Lett. 231B (1989) 530;
OPAL Collaboration, G. Alexander *et al.*, CERN-PPE/91-67 (1991), Submitted to Z. Phys. C.

[4] S. Jadach *et al.*, Z Physics at LEP1, CERN 89-08, ed. G. Altarelli *et al.*, Vol. 1 (1989) 235; CERN 89-08, Vol. 3 (1989) 69.

[5] M. Böhm, A. Denner and W. Hollik, Nucl. Phys. B304 (1988) 687;
F. A. Berends, R. Kleiss and W. Hollik, Nucl. Phys. B304 (1988) 712.

[6] R. Battacharya, J. Smith and G. Grammer, Phys. Rev. D15 (1977) 3267;
J. Smith, J. A. M. Vermaseren and G. Grammer, Phys. Rev. D15 (1977) 3280.

[7] T. Sjöstrand, Comp. Phys. Comm. 39 (1986) 347;
M. Bengtsson and T. Sjöstrand, Comp. Phys. Comm. 43 (1987) 367;
M. Bengtsson and T. Sjöstrand, Nucl. Phys. B289 (1987) 810.

[8] OPAL Collaboration, M. Akrawy *et al.*, Z. Phys. C47 (1990) 505.

[9] J. Allison *et al.*, Comp. Phys. Comm. 47 (1987) 55;
D. R. Ward, Proceedings of the MC'91 Workshop, NIKHEF, Amsterdam, 1991.

[10] G. Marchesini and B. Webber, Nucl. Phys. B310 (1988) 461;
G. Marchesini and B. Webber, Cavendish-HEP-88/7 (1988).

[11] OPAL Collaboration, G. Alexander *et al.*, Phys Lett. 264B (1991) 467.

[12] TASSO Collaboration, W. Braunschweig *et al.*, Z. Phys. C45 (1989) 193.

[13] MARK II Collaboration, G. S. Abrams *et al.*, Phys. Rev. Lett. 64 (1990) 1334.

[14] ALEPH Collaboration, D. Decamp *et al.*, Phys. Lett. 234B (1990) 209.

[15] DELPHI Collaboration, P. Abreu *et al.*, Z. Phys. C50 (1991) 185.

[16] DELPHI Collaboration, P. Abreu *et al.*, "Charged Particle Multiplicity Distributions in Restricted Rapidity Intervals in Z^0 Hadronic Decays", CERN-PPE/91-78 (1991).

[17] L3 Collaboration, B. Adeva *et al.*, "Measurement of the Inclusive Production of Neutral Pions and Charged Particles on the Z^0 Resonance", L3 preprint #25 (1991).

[18] $\gamma\gamma 2$ Collaboration, C. Bacci *et al.*, Phys. Lett. 86B (1979) 234.

[19] MARK I Collaboration, J. L. Siegrist *et al.*, Phys. Rev. D26 (1982) 969.

[20] LENA Collaboration, B. Niczyporuk *et al.*, Z. Phys. C9 (1981) 1.

[21] CLEO Collaboration, M. S. Alam *et al.*, Phys. Rev. Lett. 49 (1982) 357.

[22] JADE Collaboration, W. Bartel *et al.*, Z. Phys. C20 (1983) 187.

[23] HRS Collaboration, M. Derrick *et al.*, Phys. Rev. D34 (1986) 3304.

[24] TPC/Two-Gamma Collaboration, H. Aihara *et al.*, Phys. Lett. 134B (1987) 299.

[25] AMY Collaboration, H. W. Zheng *et al.*, Phys. Rev. D42 (1990) 737.

[26] E. Fermi *et al.*, Prog. Theor. Phys. 5 (1950) 570.

[27] H. Satz in "Current Induced Reactions"; J. G. Körner, G. Kramer and D. Schildknecht (Lecture Notes in Physics, vol. 56) Springer-Verlag, Berlin, 1975, p. 49.

[28] R. Szwed, G. Wrochna, A. K. Wròblewski, "New AMY and DELPHI Multiplicity Data and the Lognormal Distribution", Warsaw University preprint IFD/6/1990 (1990).

[29] W. Thomé *et al.*, Nucl. Phys. B129 (1977) 365.

[30] W. Furmanski, R. Petronzio, S. Pokorski, Nucl. Phys. B155 (1979) 253;
A. Bassetto, M. Ciafaloni, G. Marchesini, Phys. Lett. 83B (1979) 207;
K. Konishi, Rutherford Rep. RL 79-035 (1979);
A. H. Mueller, Phys. Lett. 104B (1981) 161; Nucl. Phys. B213 (1983) 85.

[31] A. H. Mueller, Nucl.Phys. B213 (1983) 85; ibid. B228 (1983) 351; ibid. B241 (1984) 141;
Yu. L. Dokshitzer and S. I. Troyan, preprint LNPI-922, Leningrad, 1984.

[32] B. R. Webber, Phys. Lett. 143B (1984) 501.

[33] T. T. Chou and C. N. Yang, Phys. Rev. Lett. 55 (1985) 1359; Phys. Lett. 167B (1986) 453 errata on ibid. 171B (1986) 486; ibid. 193B (1987) 531.

[34] S. Barshay, Z. Phys. C48 (1990) 453.

[35] P. Carruthers, C. C. Shih, Int. J. Mod. Phys. A2 (1987) 1447.

[36] Z. Koba, M. B. Nielsen and P. Olesen, Nucl. Phys. B40 (1972) 317.

[37] R. P. Feynman, Phys. Rev. Lett. 23(1969) 1415.

[38] A. I. Golokhvastov, Sov.J.Nucl.Phys. 27 (1978) 430; ibid. 30 (1979) 128.

[39] R. Szwed and G. Wrochna, Z. Phys. C29 (1985) 255;
A. I. Golokhvastov, Dubna preprint, JINR E2-87-484 (1987);
R. Szwed and G. Wrochna , "Scaling Predictions for Multiplicity Distributions at LEP", Warsaw University preprint IFD/3/1989 (1989).

[40] UA5 Collaboration, G. J. Alner *et al.*, Phys. Rep. 154 (1987) 247;
UA5 Collaboration, R. E. Ansorge *et al.*, Z. Phys. C43 (1989) 357.

[41] G. Wrochna, "How to fit the Lognormal Distribution", Warsaw University preprint IFD/8/1990 (1990).

[42] A. Giovannini, Z. Phys. C30 (1986) 391;
A. Giovannini and L. Van Hove, Acta Physica Polonica Vol. B19 (1988) 495;
G. Ekspong, Proc. XVI Intern. Symp. on Multiparticle Dynamics; J. Grunhaus ed. (Editions Frontieres, World Scientific, Singapore, 1985).

[43] E. D. Malaza and B. R. Webber, Phys. Lett. 149B (1984) 501;
E. D. Malaza and B. R. Webber, Nucl. Phys. B267 (1986) 702.

[44] DELPHI Collaboration, V. Uvarov, talk given at the XXVIth Rencontres de Moriond, High Energy in Hadronic Interactions, March 17-23, 1991.

whole event							
Systematic error source	$< n_{ch} >$	D	$< n_{ch} > / D$	C_2	C_3	C_4	C_5
1. Detector simulation	0.3%	0.4%	0.3%	0.06%	0.2%	0.3%	0.4%
2. Track and event selection	1.6%	2.0%	0.3%	0.06%	0.2%	0.3%	0.4%
3. Model dependence	1.1%	2.3%	3.4%	0.6%	1.9%	4.2%	7.7%
Overall systematic uncertainty	2.0%	3.1%	3.4%	0.6%	1.9%	4.2%	7.7%
single hemisphere							
Systematic error source	$< n_{ch} >$	D	$< n_{ch} > / D$	C_2	C_3	C_4	C_5
1. Detector simulation	0.2%	0.9%	0.9%	0.3%	0.7%	1.3%	1.9%
2. Track and event selection	1.5%	2.5%	1.0%	0.3%	0.7%	1.3%	1.9%
3. Model dependence	0.9%	1.4%	2.3%	0.7%	2.0%	4.0%	6.7%
Overall systematic uncertainty	1.8%	3.0%	2.7%	0.8%	2.2%	4.4%	7.2%

Table 1: Contributions to the overall systematic uncertainty on the moments of the distributions, including K^0_s and Λ decay products.

n	$P(n)$ % (whole event)	n	$P(n)$ % (single hemisphere)
2	0.0010 ± 0.0010^a	0	$0.017 \pm 0.007 \pm 0.005$
4	0.016 ± 0.020^a	1	$0.092 \pm 0.017 \pm 0.023$
6	$0.16 \pm 0.03 \pm 0.10$	2	$0.446 \pm 0.038 \pm 0.089$
8	$0.68 \pm 0.05 \pm 0.18$	3	$1.18 \pm 0.06 \pm 0.16$
10	$2.08 \pm 0.08 \pm 0.19$	4	$2.74 \pm 0.09 \pm 0.29$
12	$4.69 \pm 0.12 \pm 0.23$	5	$4.57 \pm 0.12 \pm 0.36$
14	$8.00 \pm 0.16 \pm 0.19$	6	$6.86 \pm 0.15 \pm 0.27$
16	$10.79 \pm 0.18 \pm 0.40$	7	$8.52 \pm 0.16 \pm 0.16$
18	$12.61 \pm 0.19 \pm 0.24$	8	$9.89 \pm 0.17 \pm 0.61$
20	$12.85 \pm 0.20 \pm 0.34$	9	$10.02 \pm 0.17 \pm 0.31$
22	$11.83 \pm 0.19 \pm 0.20$	10	$9.72 \pm 0.17 \pm 0.30$
24	$9.99 \pm 0.17 \pm 0.35$	11	$8.68 \pm 0.16 \pm 0.27$
26	$7.85 \pm 0.15 \pm 0.14$	12	$7.64 \pm 0.15 \pm 0.17$
28	$5.95 \pm 0.13 \pm 0.17$	13	$6.42 \pm 0.13 \pm 0.17$
30	$4.35 \pm 0.11 \pm 0.17$	14	$5.26 \pm 0.12 \pm 0.15$
32	$2.97 \pm 0.09 \pm 0.09$	15	$4.24 \pm 0.11 \pm 0.08$
34	$2.02 \pm 0.08 \pm 0.09$	16	$3.33 \pm 0.10 \pm 0.05$
36	$1.29 \pm 0.06 \pm 0.11$	17	$2.62 \pm 0.08 \pm 0.07$
38	$0.81 \pm 0.05 \pm 0.06$	18	$2.02 \pm 0.07 \pm 0.07$
40	$0.47 \pm 0.04 \pm 0.05$	19	$1.55 \pm 0.07 \pm 0.11$
42	$0.26 \pm 0.03 \pm 0.04$	20	$1.18 \pm 0.06 \pm 0.08$
44	$0.17 \pm 0.02 \pm 0.05$	21	$0.856 \pm 0.050 \pm 0.069$
46	$0.089 \pm 0.016 \pm 0.038$	22	$0.646 \pm 0.043 \pm 0.052$
48	$0.042 \pm 0.011 \pm 0.020$	23	$0.462 \pm 0.036 \pm 0.064$
50	$0.025 \pm 0.009 \pm 0.015$	24	$0.326 \pm 0.032 \pm 0.051$
52	$0.011 \pm 0.007 \pm 0.007$	25	$0.250 \pm 0.029 \pm 0.051$
54	$0.004 \pm 0.004 \pm 0.004$	26	$0.164 \pm 0.023 \pm 0.050$
		27	$0.103 \pm 0.017 \pm 0.041$
		28	$0.067 \pm 0.013 \pm 0.028$
		29	$0.046 \pm 0.012 \pm 0.021$
		30	$0.030 \pm 0.009 \pm 0.014$
		31	$0.017 \pm 0.006 \pm 0.005$
		32	$0.011 \pm 0.005 \pm 0.005$
		33	$0.0052 \pm 0.0038 \pm 0.0050$
		34	$0.0020 \pm 0.0020 \pm 0.0023$

[a] not measured, taken from JETSET 7.2

Table 2 (a): Charged multiplicity distributions $P(n) = \frac{1}{N_{ev}} \frac{dN}{dn}$ (%) for the whole event and for a single hemisphere. Statistical (first) and systematic (second) uncertainties are listed separately. The fraction of events at multiplicities n=2 and n=4 in the whole event distribution are the JETSET model predictions and their associated overall uncertainties correspond to the difference between the JETSET and HERWIG predictions. These two points have not been used when fitting analytical parameterisations to the shape of the distribution.

n	$P(n)$ % *(whole event)*	n	$P(n)$ % *(single hemisphere)*
2	0.0054 ± 0.0054^a	0	$0.046 \pm 0.015 \pm 0.014$
4	0.060 ± 0.070^a	1	$0.192 \pm 0.025 \pm 0.050$
6	$0.39 \pm 0.04 \pm 0.24$	2	$0.818 \pm 0.050 \pm 0.16$
8	$1.52 \pm 0.07 \pm 0.40$	3	$2.02 \pm 0.08 \pm 0.28$
10	$4.02 \pm 0.11 \pm 0.36$	4	$4.16 \pm 0.11 \pm 0.46$
12	$7.54 \pm 0.15 \pm 0.38$	5	$6.38 \pm 0.14 \pm 0.51$
14	$11.06 \pm 0.18 \pm 0.27$	6	$8.84 \pm 0.16 \pm 0.35$
16	$13.28 \pm 0.20 \pm 0.49$	7	$10.13 \pm 0.17 \pm 0.20$
18	$13.78 \pm 0.20 \pm 0.28$	8	$10.91 \pm 0.18 \pm 0.65$
20	$12.63 \pm 0.19 \pm 0.33$	9	$10.32 \pm 0.17 \pm 0.32$
22	$10.53 \pm 0.17 \pm 0.21$	10	$9.44 \pm 0.16 \pm 0.29$
24	$8.13 \pm 0.15 \pm 0.28$	11	$8.03 \pm 0.15 \pm 0.25$
26	$6.01 \pm 0.13 \pm 0.12$	12	$6.75 \pm 0.14 \pm 0.15$
28	$4.13 \pm 0.11 \pm 0.12$	13	$5.37 \pm 0.12 \pm 0.14$
30	$2.74 \pm 0.09 \pm 0.11$	14	$4.27 \pm 0.11 \pm 0.12$
32	$1.76 \pm 0.07 \pm 0.05$	15	$3.28 \pm 0.09 \pm 0.06$
34	$1.08 \pm 0.05 \pm 0.05$	16	$2.49 \pm 0.08 \pm 0.04$
36	$0.62 \pm 0.04 \pm 0.05$	17	$1.85 \pm 0.07 \pm 0.05$
38	$0.36 \pm 0.03 \pm 0.03$	18	$1.40 \pm 0.06 \pm 0.05$
40	$0.21 \pm 0.03 \pm 0.02$	19	$1.02 \pm 0.05 \pm 0.07$
42	$0.10 \pm 0.02 \pm 0.02$	20	$0.730 \pm 0.046 \pm 0.044$
44	$0.055 \pm 0.013 \pm 0.016$	21	$0.510 \pm 0.038 \pm 0.041$
46	$0.028 \pm 0.011 \pm 0.012$	22	$0.353 \pm 0.031 \pm 0.028$
48	$0.015 \pm 0.009 \pm 0.007$	23	$0.232 \pm 0.025 \pm 0.032$
50	$0.005 \pm 0.004 \pm 0.003$	24	$0.160 \pm 0.022 \pm 0.026$
52	$0.002 \pm 0.002 \pm 0.001$	25	$0.109 \pm 0.019 \pm 0.022$
		26	$0.068 \pm 0.014 \pm 0.020$
		27	$0.046 \pm 0.012 \pm 0.018$
		28	$0.030 \pm 0.010 \pm 0.013$
		29	$0.013 \pm 0.007 \pm 0.006$
		30	$0.012 \pm 0.006 \pm 0.006$
		31	$0.0058 \pm 0.0040 \pm 0.002$
		32	$0.0052 \pm 0.0052 \pm 0.003$

[a] not measured, taken from JETSET 7.2

Table 2 (b): Charged multiplicity distributions $P(n) = \frac{1}{N_{ev}} \frac{dN}{dn}$ (%) for the whole event and for a single hemisphere. Contributions to the charged multiplicities from K^0_s and Λ decays have been subtracted.

Moment	*whole event*	*single hemisphere*
$< n_{ch} >$	$21.40 \pm 0.02 \pm 0.43$	$10.70 \pm 0.02 \pm 0.19$
D	$6.49 \pm 0.02 \pm 0.20$	$4.40 \pm 0.01 \pm 0.13$
$< n_{ch} > /D$	$3.30 \pm 0.01 \pm 0.11$	$2.431 \pm 0.008 \pm 0.064$
C_2	$1.0920 \pm 0.0005 \pm 0.007$	$1.169 \pm 0.001 \pm 0.009$
C_3	$1.293 \pm 0.002 \pm 0.025$	$1.563 \pm 0.003 \pm 0.035$
C_4	$1.649 \pm 0.004 \pm 0.07$	$2.348 \pm 0.010 \pm 0.10$
C_5	$2.251 \pm 0.010 \pm 0.17$	$3.899 \pm 0.028 \pm 0.28$

Table 3 (a): Moments of the charged multiplicity distributions for the whole event and for a single hemisphere. The values contain the contributions from K^0_s and Λ decays. The first error is statistical, the second is systematic.

Moment	*whole event*	*single hemisphere*
$< n_{ch} >$	$19.41 \pm 0.02 \pm 0.40$	$9.69 \pm 0.01 \pm 0.18$
D	$6.06 \pm 0.02 \pm 0.16$	$4.10 \pm 0.01 \pm 0.12$
$< n_{ch} > /D$	$3.20 \pm 0.01 \pm 0.10$	$2.364 \pm 0.008 \pm 0.066$
C_2	$1.0975 \pm 0.0005 \pm 0.006$	$1.179 \pm 0.001 \pm 0.010$
C_3	$1.311 \pm 0.002 \pm 0.02$	$1.597 \pm 0.004 \pm 0.041$
C_4	$1.694 \pm 0.004 \pm 0.05$	$2.439 \pm 0.011 \pm 0.12$
C_5	$2.349 \pm 0.011 \pm 0.12$	$4.133 \pm 0.033 \pm 0.34$

Table 3 (b): Moments of the charged multiplicity distributions for the whole event and for a single hemisphere. Contributions to the charged multiplicities from K^0_s and Λ decays have been subtracted.

Figure Captions

Figure 1 The observed (uncorrected) multiplicity distributions (solid points) for the whole event and for a single hemisphere. Also shown, as histograms, are the predictions of the JETSET 7.2 (a,b) and HERWIG 5.0 (c,d) parton shower models, which include simulation of the detector.

Figure 2 The corrected multiplicity distributions (solid points) for (a) the whole event and for (b) a single hemisphere. The plotted errors contain statistical and systematic uncertainties. The contributions from K^0_s and Λ charged decay products are included. Also shown are the predictions from the Lund parton shower model JETSET (continuous line).

Figure 3 The energy dependence of the mean charged multiplicity measured in e^+e^- annihilations. All measurements include contributions from K^0_s and Λ decays. The plotted errors are the quadratic sum of statistical and systematic uncertainties, except for the measurements done by the $\gamma\gamma 2$ and MARK I collaborations.

Figure 4 The energy dependence of $< n_{ch} > /D$ (a) and of the normalised moments C_k(b) computed from the whole event multiplicity distribution. All these values contain the contribution from K^0_s and Λ decays.

Figure 5 Same as in Fig. 4 but for a single hemisphere.

Figure 6 The ratio $R = (< n_{ch} > /D)^{Whole}_{event}/(< n_{ch} > /D)^{Single}_{Hem.}$ determined from a study of events with different mean sphericity. Each point is plotted in correspondence with the sphericity cut used. As an example, the point at 0.3 on the horizontal axis corresponds to events whose measured sphericity was smaller than 0.3. The errors shown are statistical only and are not independent.

Figure 7 Multiplicity distributions for the whole event measured in e^+e^- annihilations at different energies plotted in the KNO form. The plotted errors correspond to statistical and systematic errors added in quadrature.

Figure 8 Graphical test of the KNO-G scaling. The same data presented in Fig. 7 are plotted in terms of the variable $S_n = \sum_{k=n}^{\infty} P_k$ as a function of the scaled variable $\tilde{z} = n/ < \bar{n} >$.

Figure 9 Results from the fit (continuous line) of a Γ function (Eq. 10) to the corrected multiplicity distribution measured for the whole event (black points). The same distribution is shown both on linear and logarithmic scale separately. Multiplicities $n_{ch} = 2$ and $n_{ch} = 4$ were not considered. On the top part of the figure we show the deviations of the analytical predictions from the measured points, plotted in units of the overall experimental uncertainty. Error bars represent one of these units.

Figure 10 Same as in Fig. 9 but for a fit performed assuming a Lognormal parameterisation (Eq. 11).

Figure 11 Results from the fit to the charged multiplicity for the whole event using a Negative Binomial Distribution.

Figure 12 Same as in Fig. 11 but for a single hemisphere.

Figure 13 Study of the multiplicity shape for events selected according to their measured sphericity. The corrected multiplicity distribution for the whole event (solid points) of the inclusive sample is shown in (a), both on a linear and a logarithmic scale, together with the results obtained by fitting the experimental points to a Modified Poissonian distribution (continuous line, Eq. 15) and to a NBD (dot-dashed line, Eq. 13). In (b) and (c) the distributions are shown for events whose measured sphericity was smaller than 0.15 and 0.03, respectively.

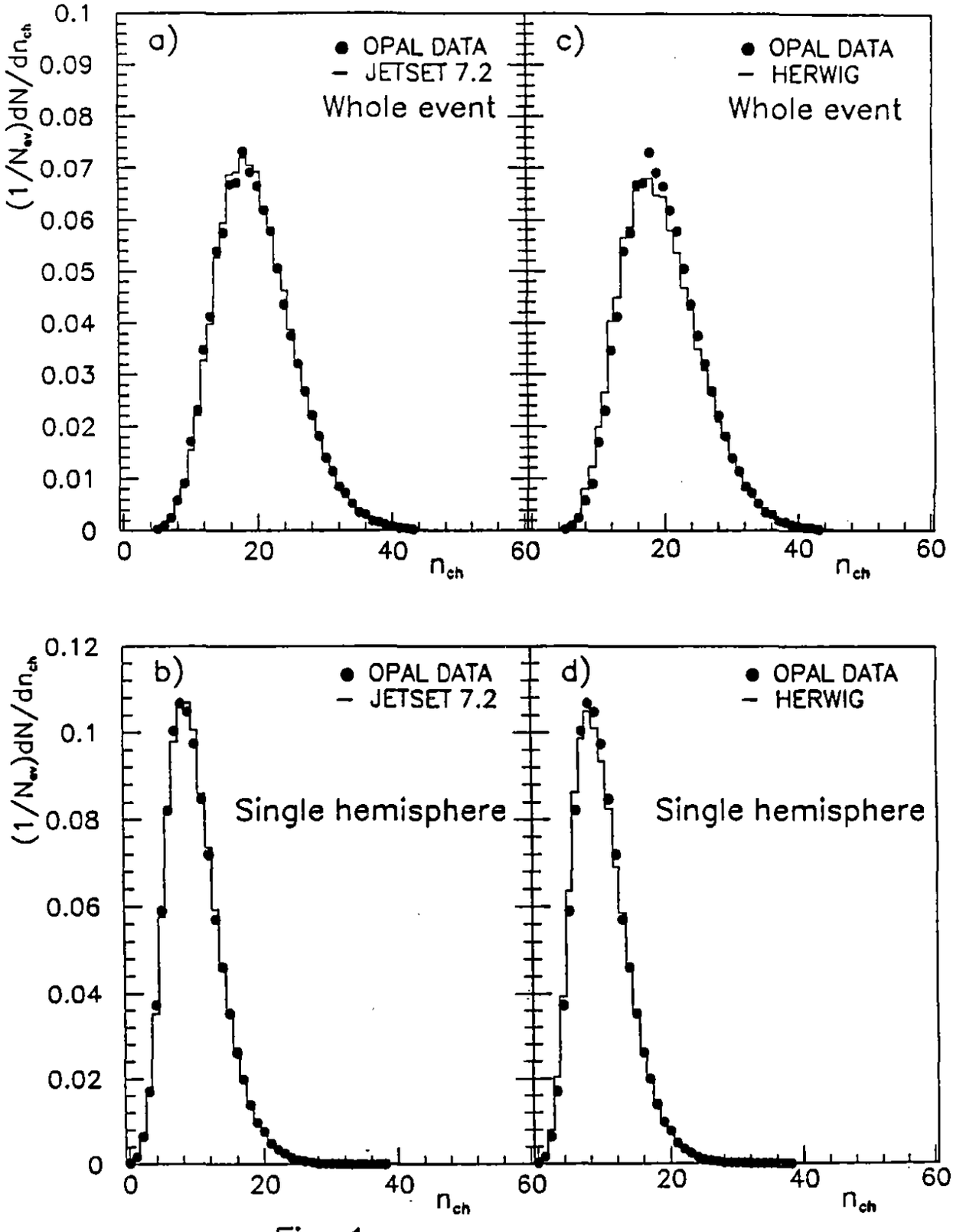
a)
OPAL DATA
JETSET 7.2
Whole event
c)
OPAL DATA
HERWIG
Whole event
b)
OPAL DATA
JETSET 7.2
Single hemisphere
d)
OPAL DATA
HERWIG
Single hemisphere
$(1/N_{ev})dN/dn_{ch}$
n_{ch}

Fig. 1

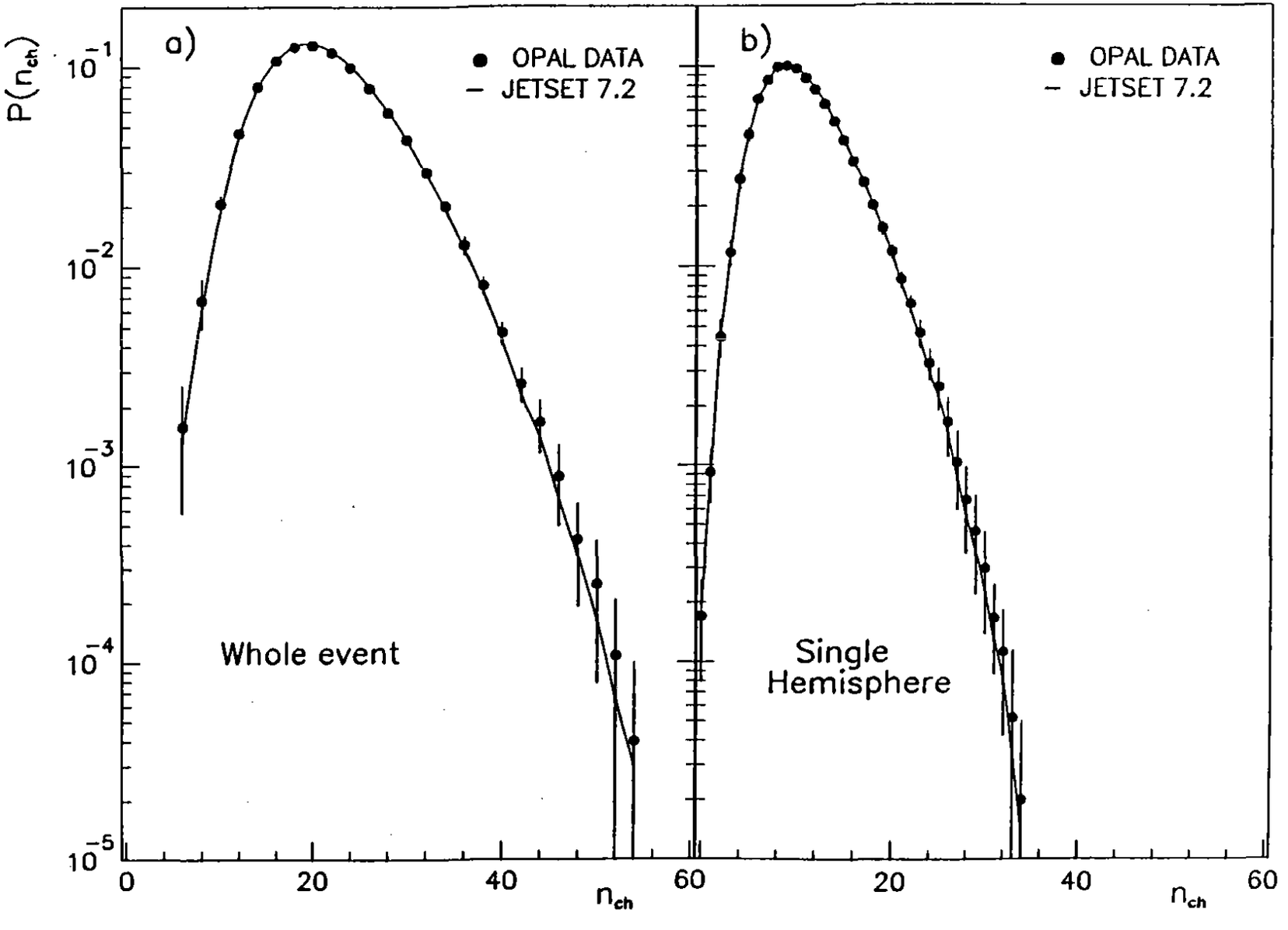
a)
b)
OPAL DATA
JETSET 7.2
$P(n_{ch})$
10^{-1}
10^{-2}
10^{-3}
10^{-4}
10^{-5}
Whole event
Single
Hemisphere
0
20
40
60
n_{ch}

Fig. 2

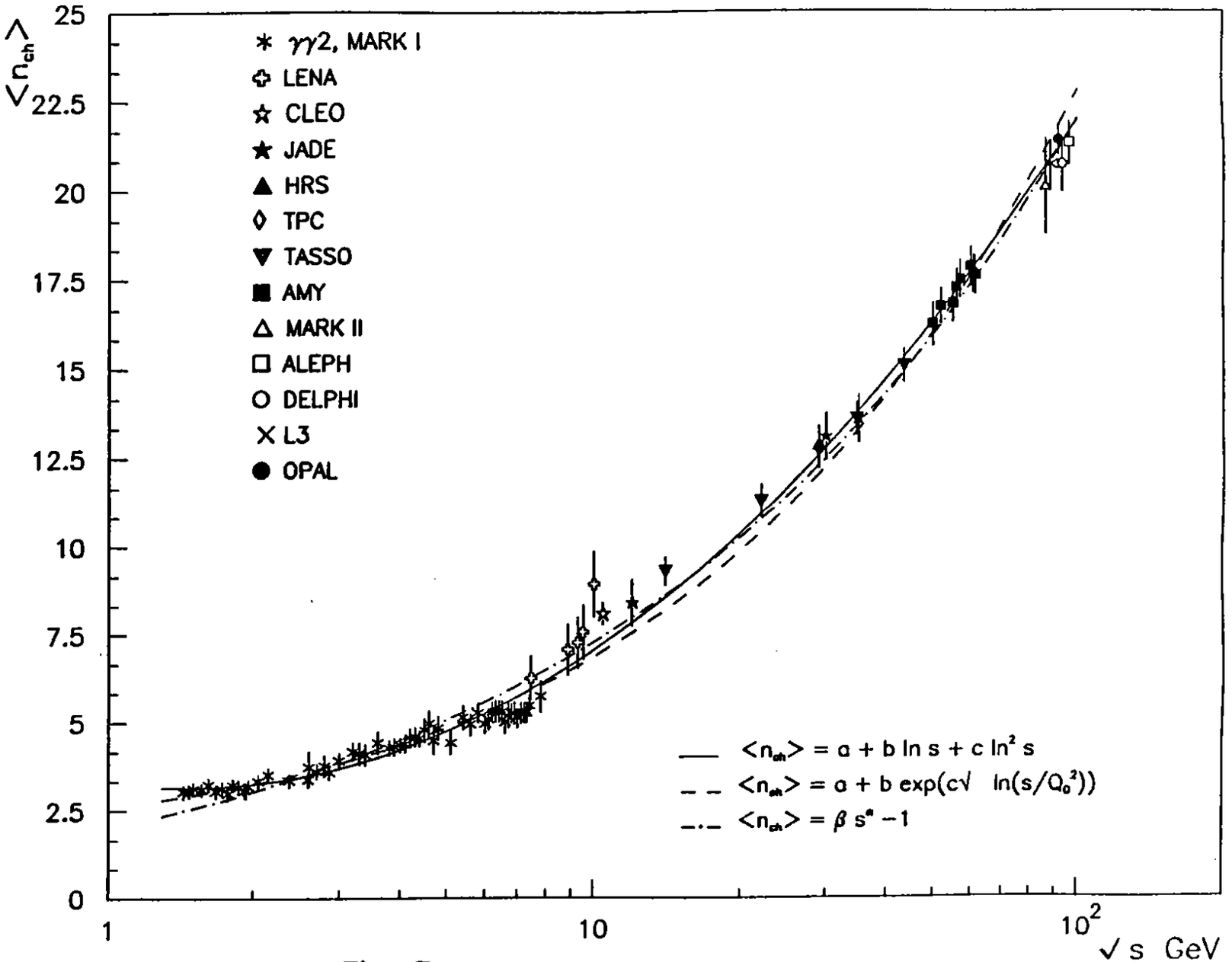
$\langle n_{ch} \rangle$
25
22.5
20
17.5
15
12.5
10
7.5
5
2.5
0
1
10
10^2
$\sqrt{s}$ GeV
* γγ2, MARK I
LENA
CLEO
JADE
HRS
TPC
TASSO
AMY
MARK II
ALEPH
DELPHI
L3
OPAL
$\langle n_{ch} \rangle = a + b \ln s + c \ln^2 s$
$\langle n_{ch} \rangle = a + b \exp(c\sqrt{\ln(s/Q_0^2)})$
$\langle n_{ch} \rangle = \beta s^{\alpha} - 1$

Fig. 3

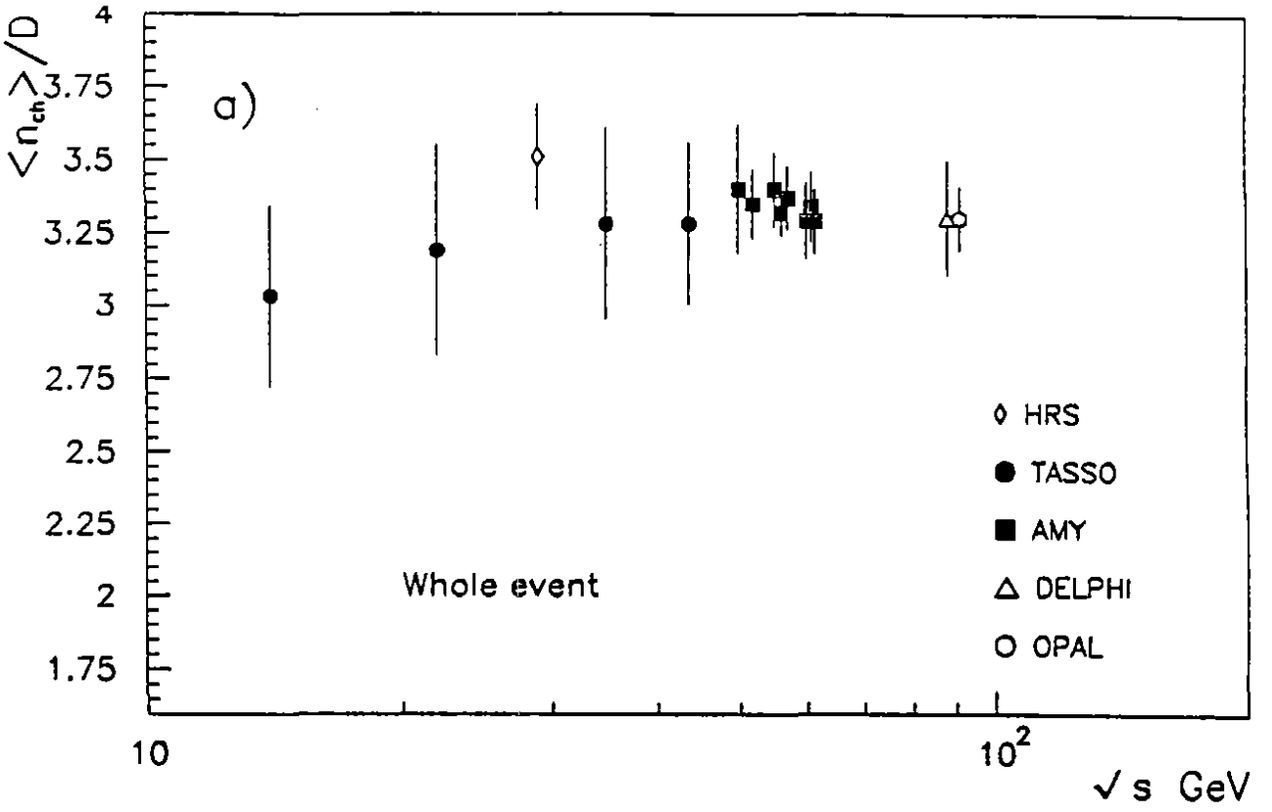
a)
$\langle n_{ch} \rangle / D$
4
3.75
3.5
3.25
3
2.75
2.5
2.25
2
1.75
Whole event
HRS
TASSO
AMY
DELPHI
OPAL
10
10^2
$\sqrt{s}$ GeV

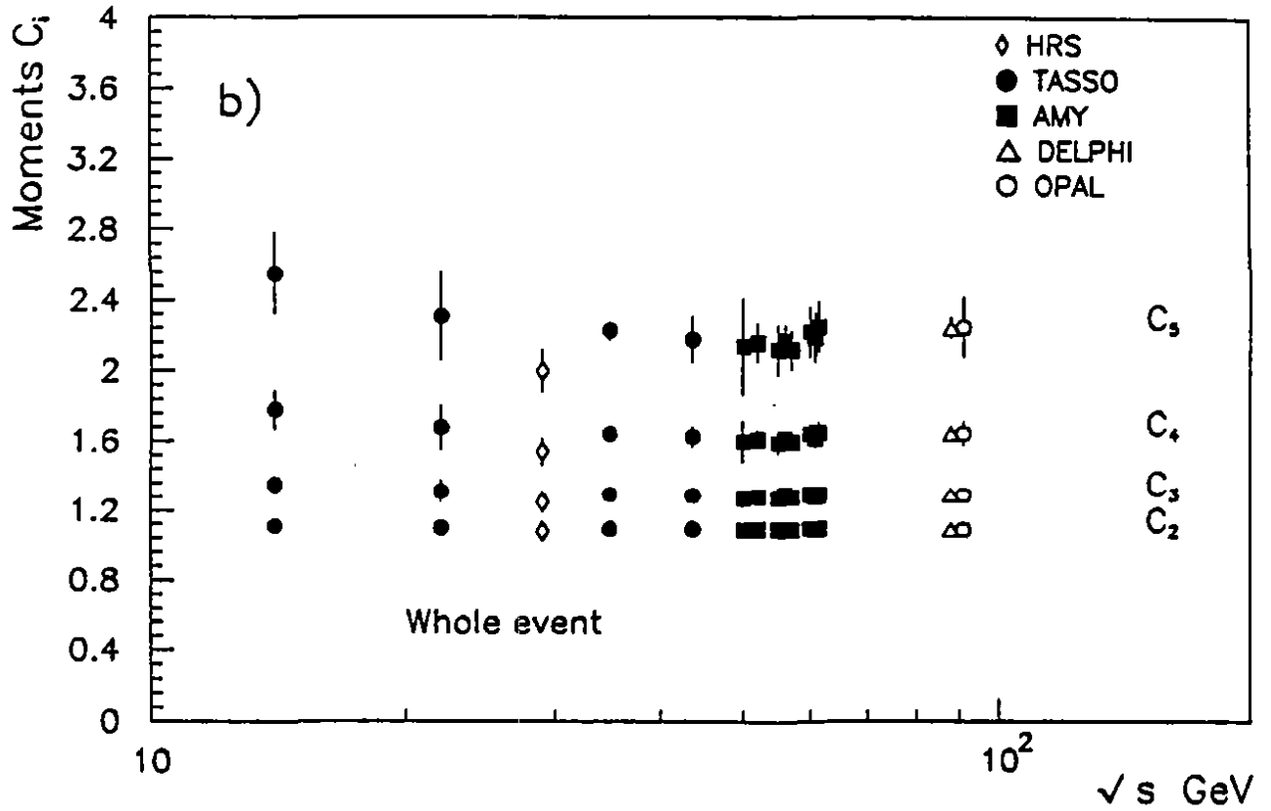
b)
Moments C_i
4
3.6
3.2
2.8
2.4
2
1.6
1.2
0.8
0.4
0
Whole event
HRS
TASSO
AMY
DELPHI
OPAL
C_5
C_4
C_3
C_2
10
10^2
$\sqrt{s}$ GeV

Fig. 4

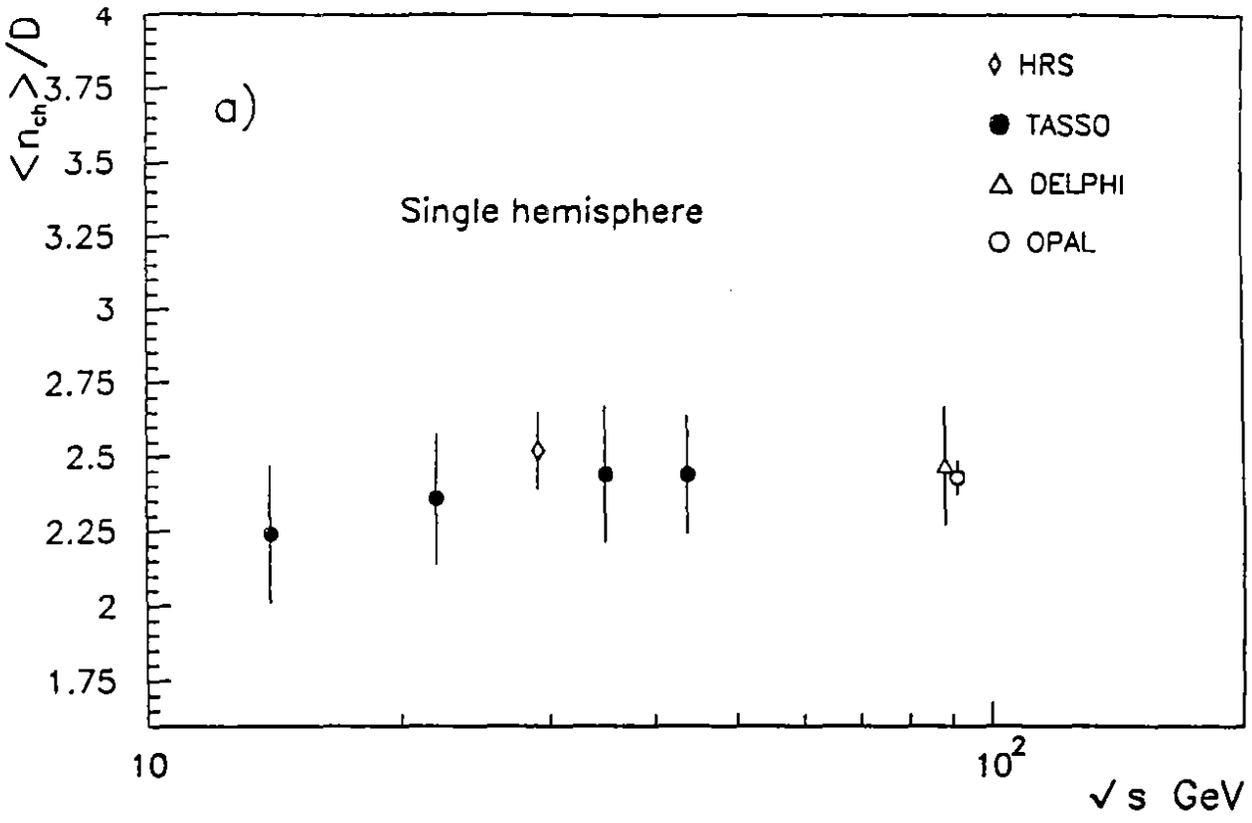
a)
Single hemisphere
HRS
TASSO
DELPHI
OPAL
$\langle n_{ch} \rangle / D$
4
3.75
3.5
3.25
3
2.75
2.5
2.25
2
1.75
10
10^2
$\sqrt{s}$ GeV

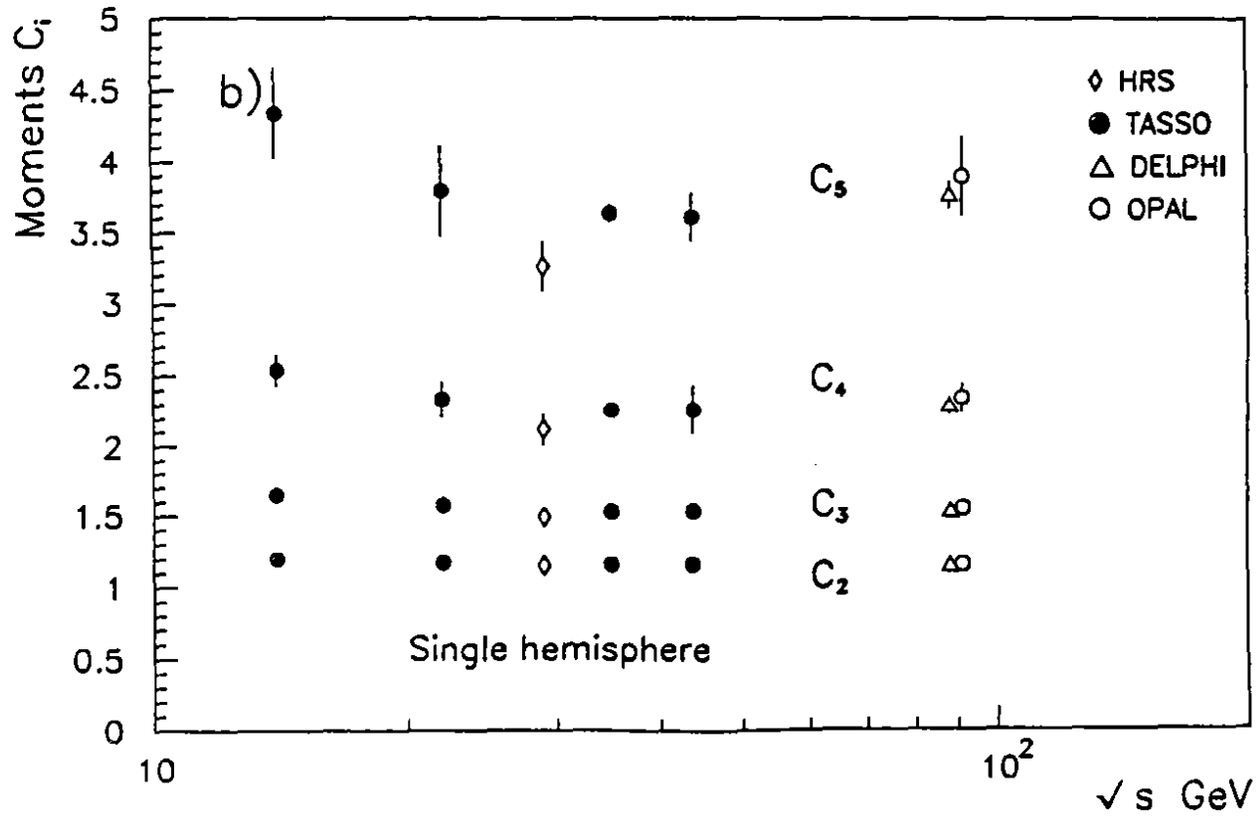
b)
Single hemisphere
HRS
TASSO
DELPHI
OPAL
C_5
C_4
C_3
C_2
Moments C_i
5
4.5
4
3.5
3
2.5
2
1.5
1
0.5
0
10
10^2
$\sqrt{s}$ GeV

Fig. 5

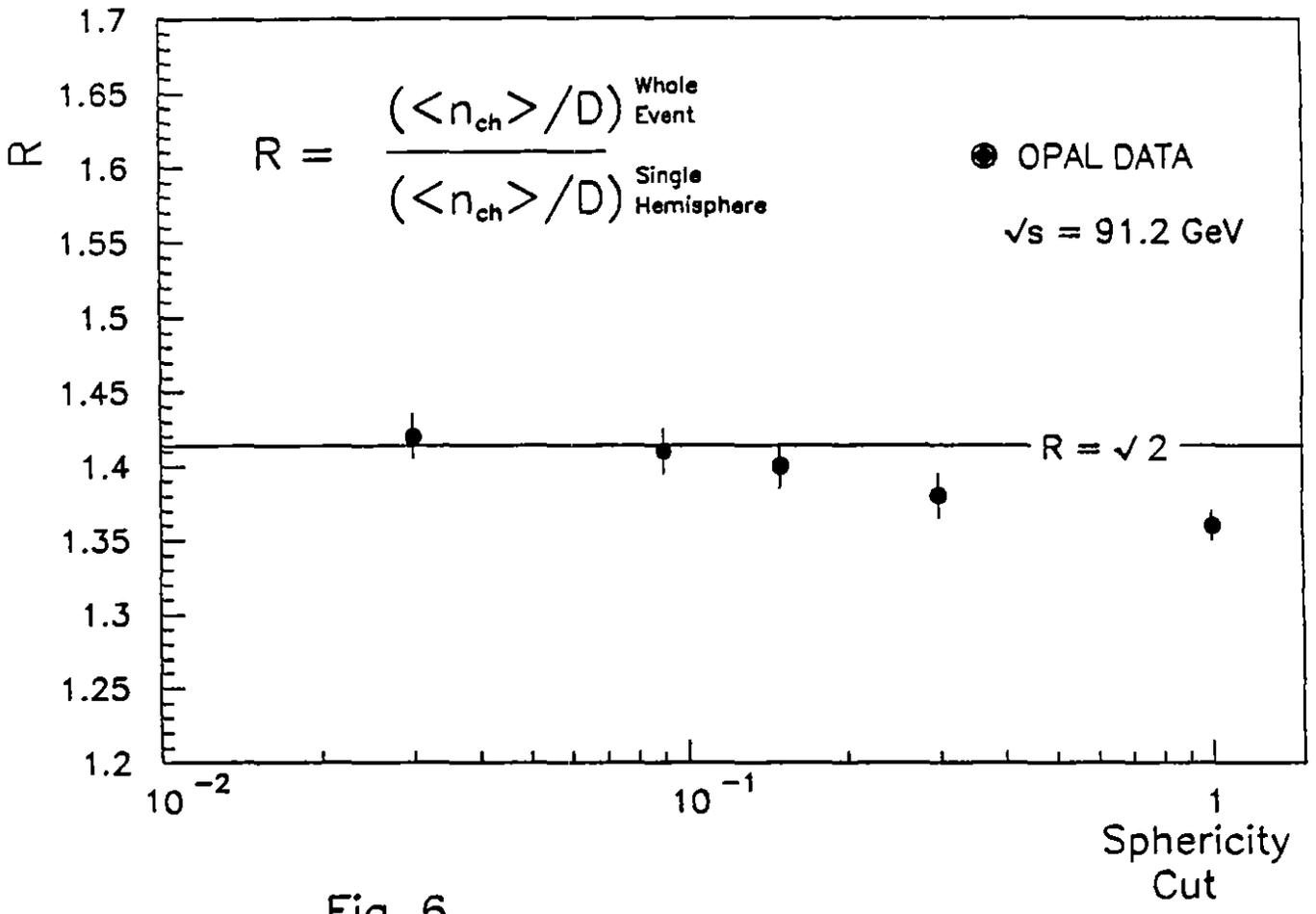
R
1.7
1.65
1.6
1.55
1.5
1.45
1.4
1.35
1.3
1.25
1.2
R = (<n_ch>/D) Whole Event / (<n_ch>/D) Single Hemisphere
OPAL DATA
√s = 91.2 GeV
R = √2
10^-2
10^-1
1
Sphericity Cut

Fig. 6

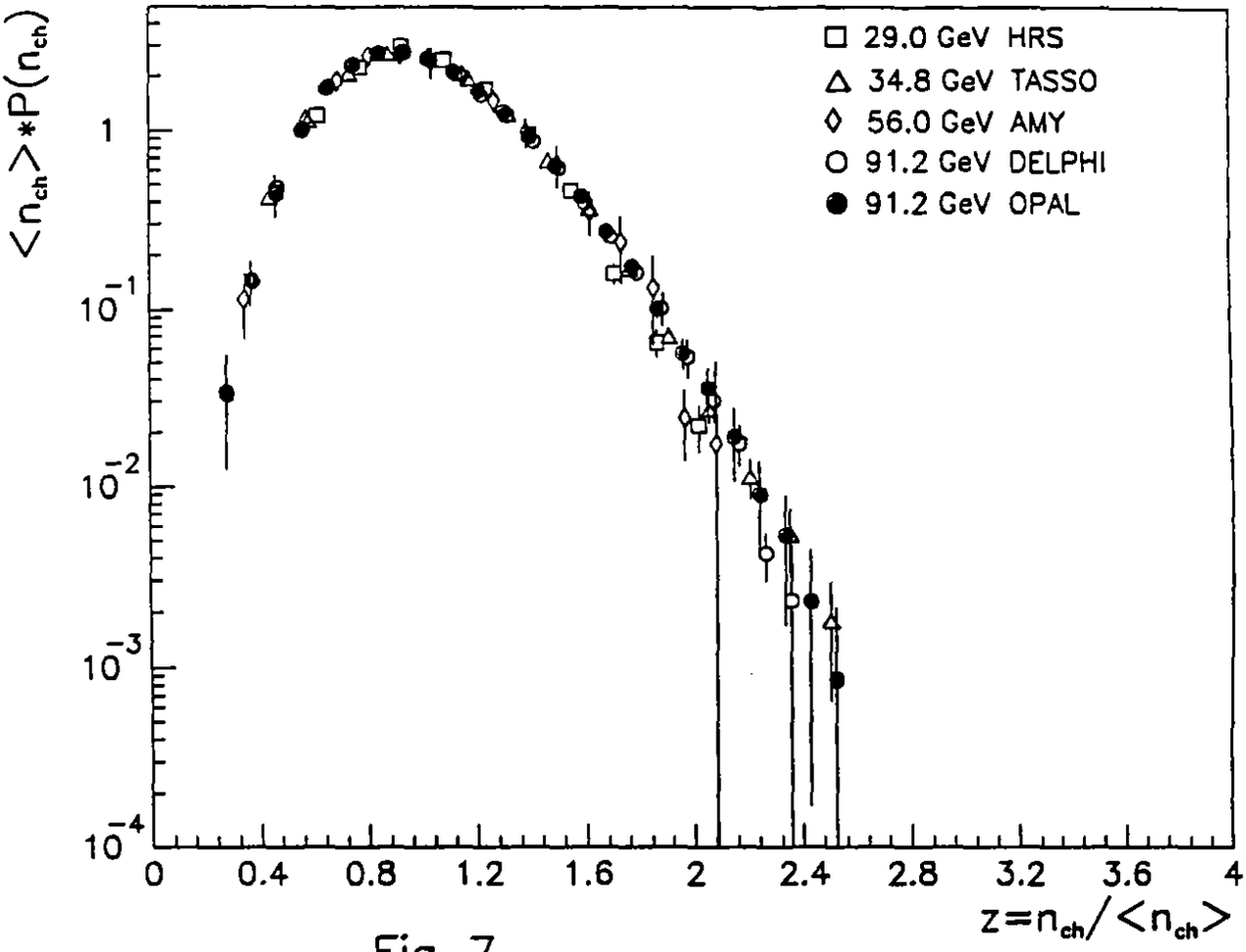
$\langle n_{ch}\rangle * P(n_{ch})$
29.0 GeV HRS
34.8 GeV TASSO
56.0 GeV AMY
91.2 GeV DELPHI
91.2 GeV OPAL
$z = n_{ch}/\langle n_{ch}\rangle$

Fig. 7

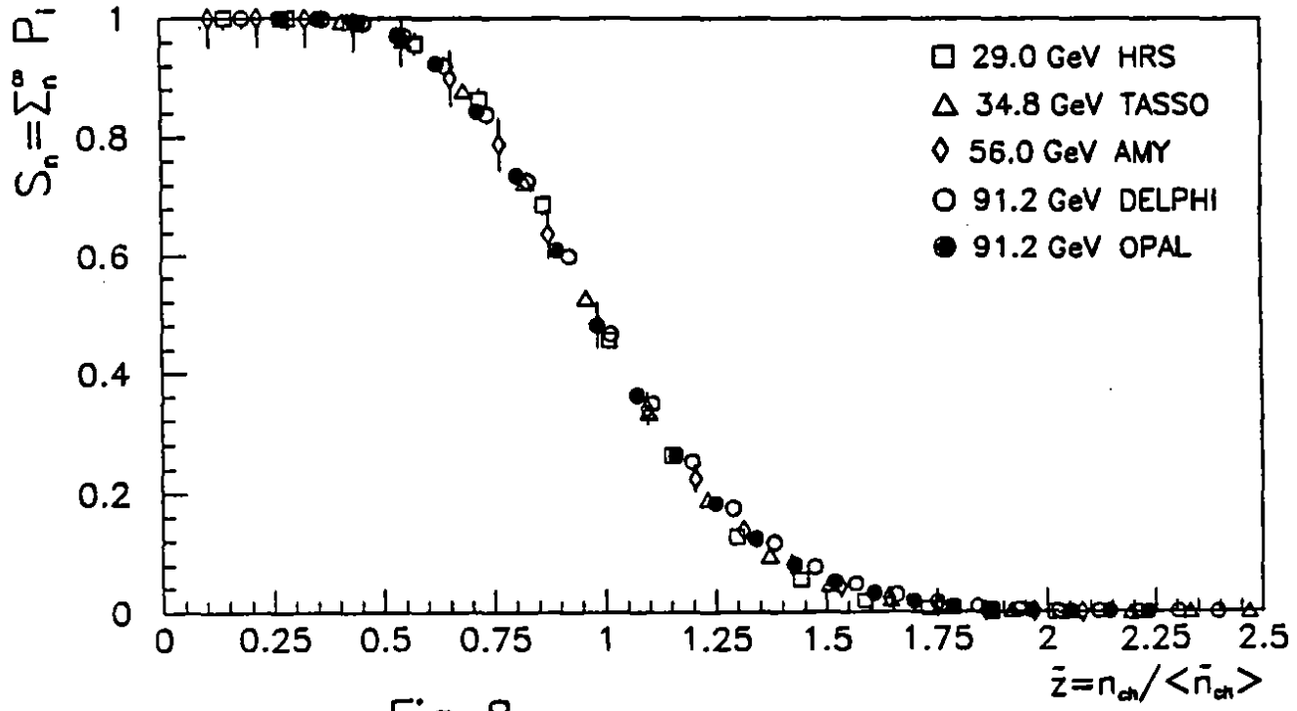
$S_n \equiv \sum_n^8 P_i$
29.0 GeV HRS
34.8 GeV TASSO
56.0 GeV AMY
91.2 GeV DELPHI
91.2 GeV OPAL
$\tilde{z} = n_{ch}/\langle \tilde{n}_{ch}\rangle$

Fig. 8

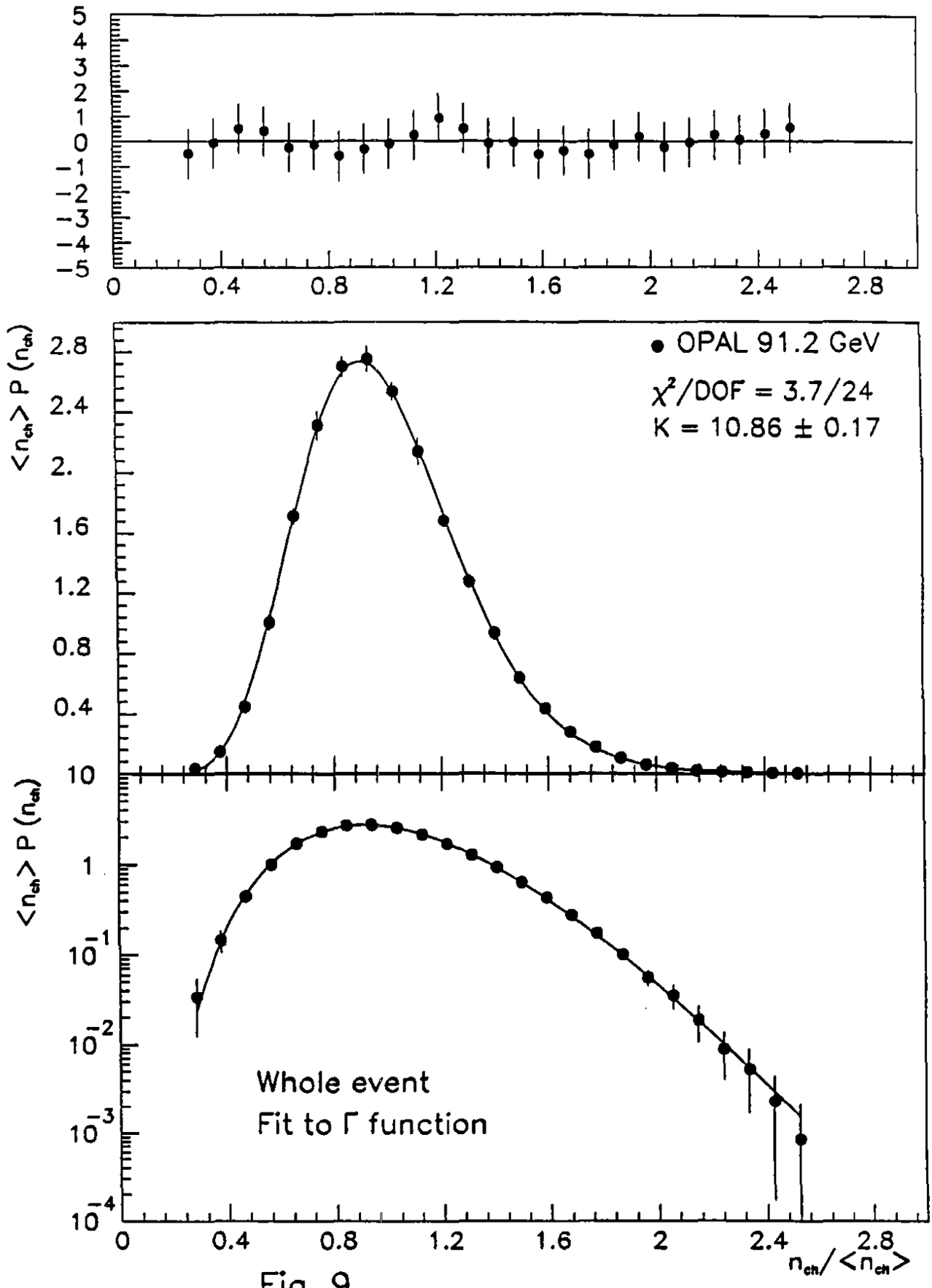
OPAL 91.2 GeV
χ^2/DOF = 3.7/24
K = 10.86 ± 0.17
$\langle n_{ch} \rangle P(n_{ch})$
Whole event
Fit to Γ function
$n_{ch}/\langle n_{ch} \rangle$

Fig. 9

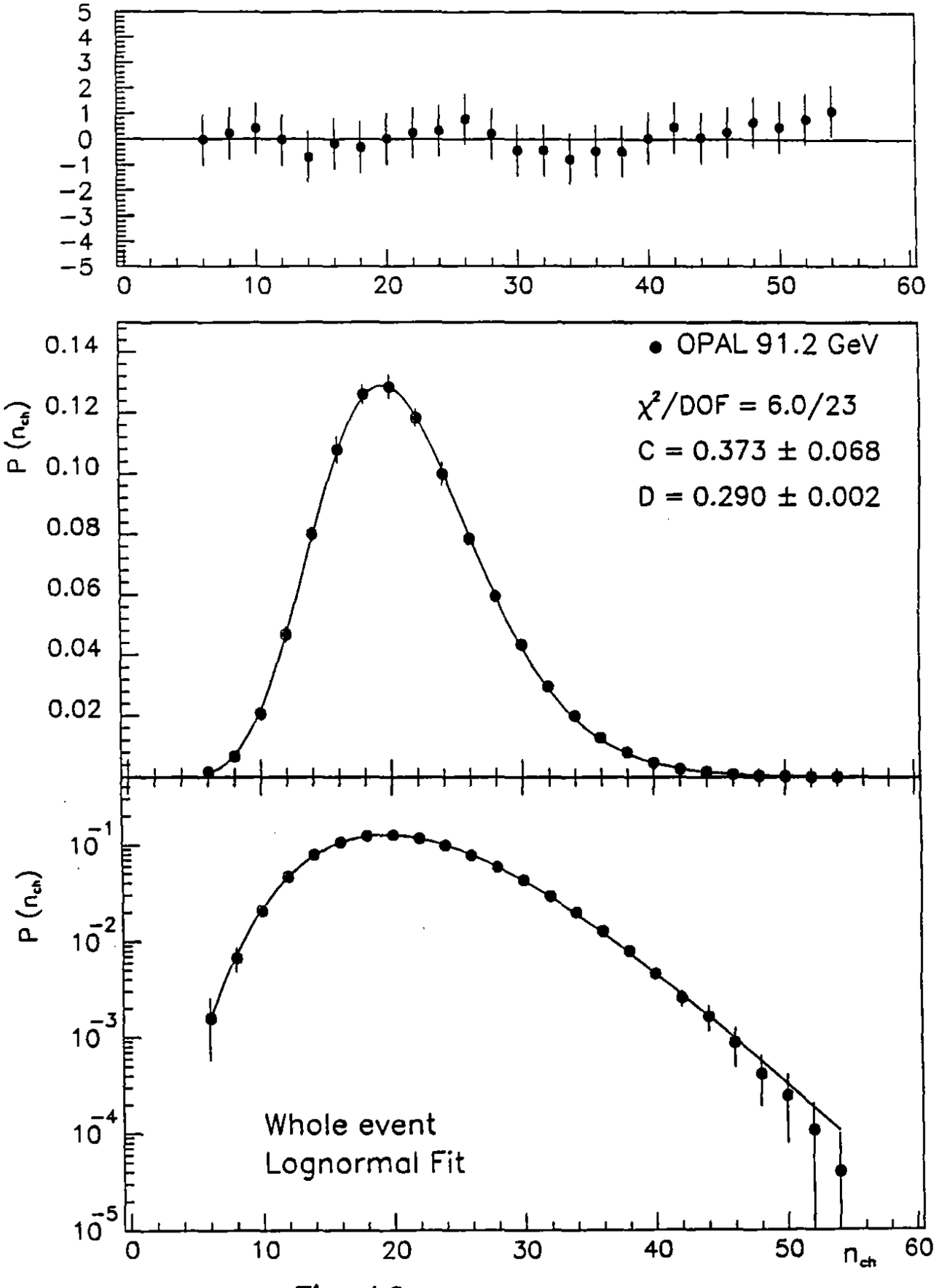
OPAL 91.2 GeV
χ^2/DOF = 6.0/23
C = 0.373 ± 0.068
D = 0.290 ± 0.002
P (n_{ch})
Whole event
Lognormal Fit
n_{ch}

Fig. 10

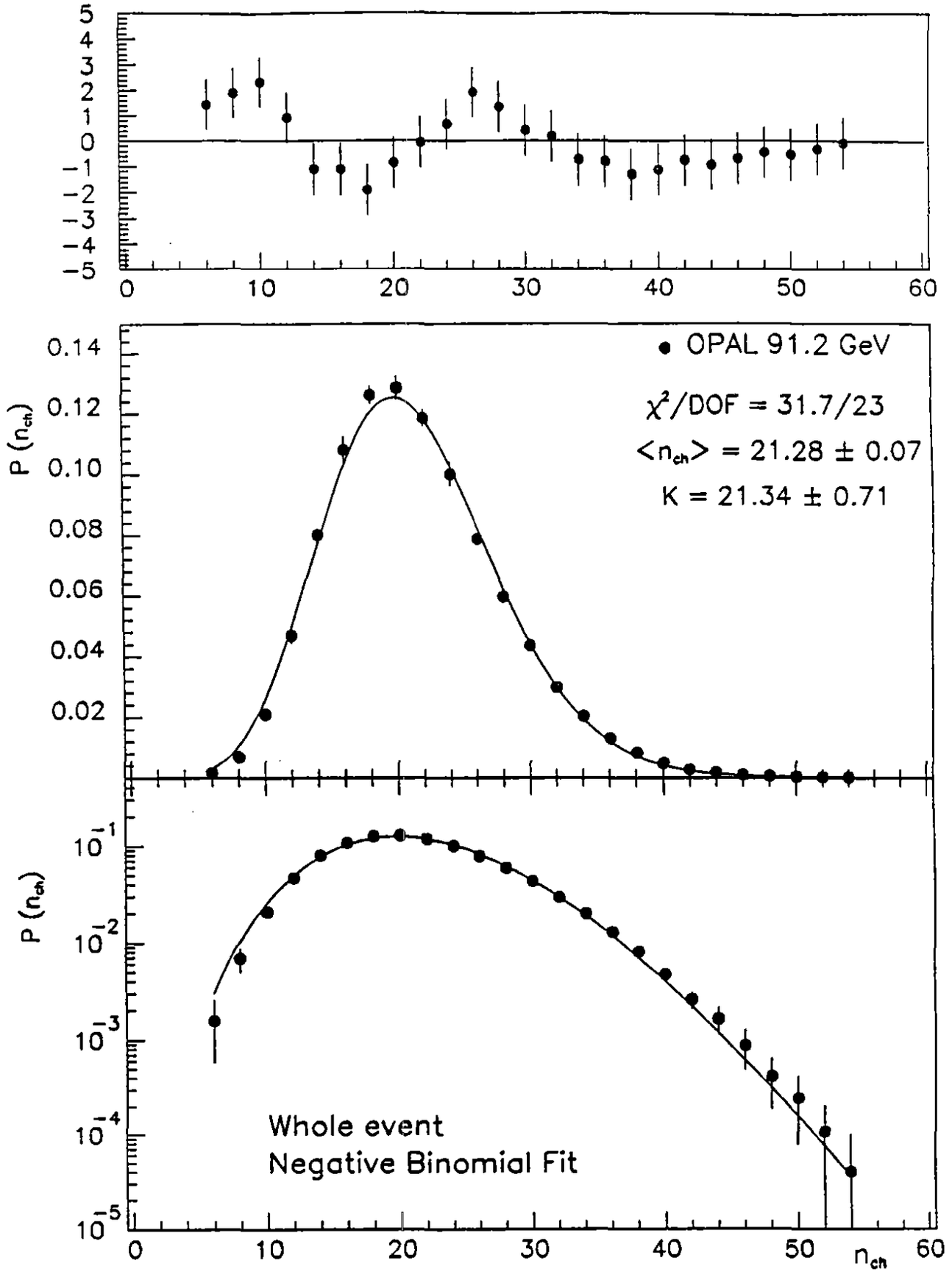
OPAL 91.2 GeV
χ^2/DOF = 31.7/23
<n_{ch}> = 21.28 ± 0.07
K = 21.34 ± 0.71
P (n_{ch})
Whole event
Negative Binomial Fit
n_{ch}

Fig. 11

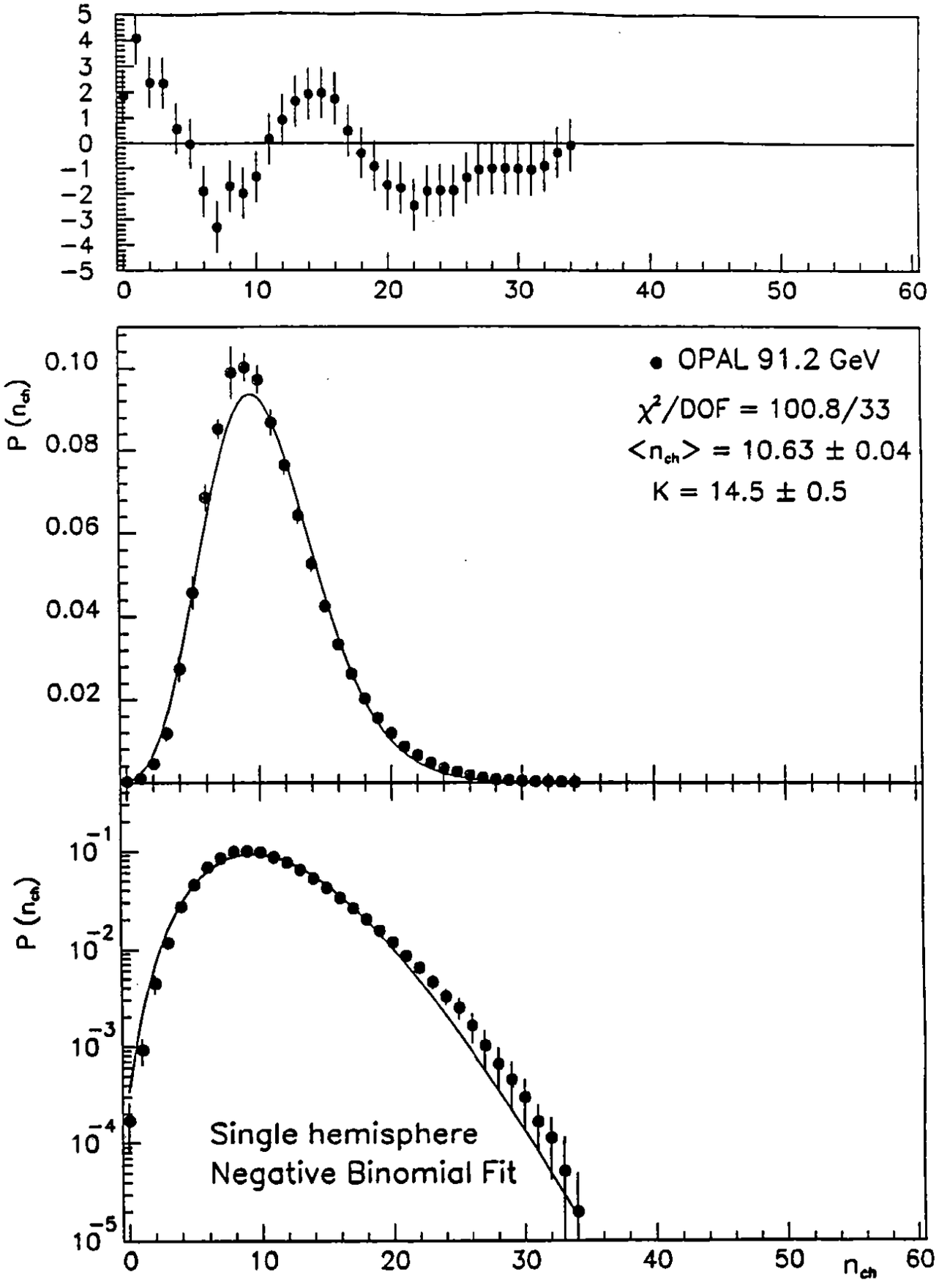
OPAL 91.2 GeV
χ^2/DOF = 100.8/33
$\langle n_{ch} \rangle$ = 10.63 ± 0.04
K = 14.5 ± 0.5
P (n_{ch})
Single hemisphere
Negative Binomial Fit
n_{ch}

Fig. 12

Imprimé au CERN. Prix: 1.15 Fr.

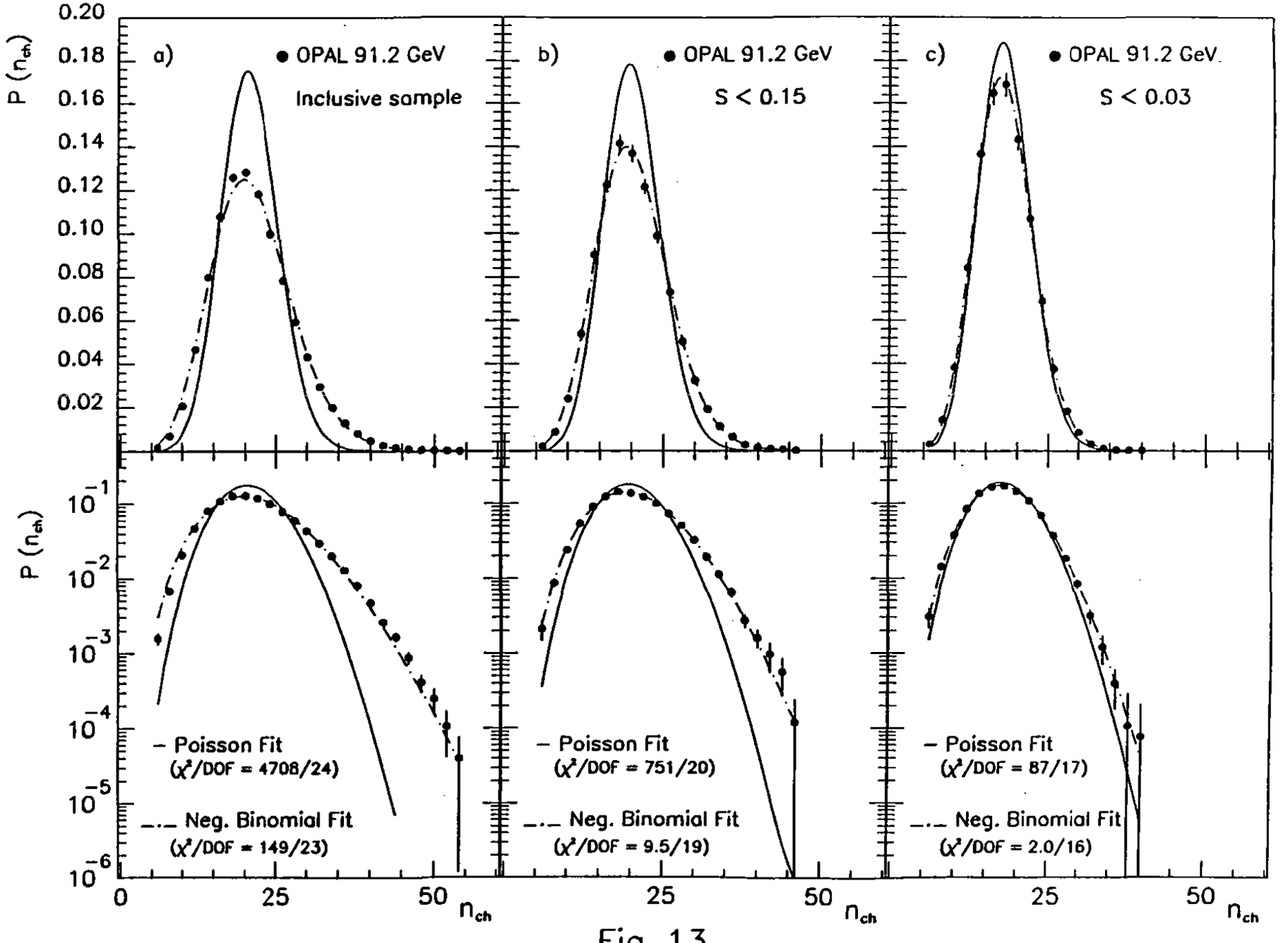

Fig. 13